THERMAL MANAGEMENT AND CHARACTERIZATION OF LIGHT-EMITTING DIODES

Susu Yan

Submitted to Mount Holyoke College in partial fulfillment of the requirements for the degree of Bachelor of Arts with Honor

Janice Hudgings, Mount Holyoke College
Thesis Advisor

May 2, 2010

Abstract

Light-emitting diodes (LEDs) are promising electronic devices used in various lighting system, such as traffic signals, large screen displays with high brightnesses, sources of general illumination. Currently, LEDs are increasingly used for everyday purposes due to their multiple advantages, which include low energy consumption, long life time and solid state high power lighting. However, temperature plays an important role in the function of LEDs and affects their performance and reliability. As the heat in LEDs escalates, several key characteristics may alter; the forward voltage may decrease, the optical wavelength may shift, and LEDs' output light may change color. Therefore, thermal management and full characterization of LEDs have been investigated to examine the effect of heat on LEDs.

In this work, we measure the thermal distribution inside the operating LED, both laterally and vertically by using thermoreflectance microscopy and two traditional measurements, in order to better understand the thermal performance of the LED.

Thermoreflectance microscopy is used to provide the first high resolution 2-Dimensional temperature distribution across the surface of the operating LED. This technique uses a CCD camera to measure the change in reflectivity (ΔR) of the test device in response to a change in temperature (ΔT):

$$\frac{\Delta R}{R} = \left(\frac{1}{R}\frac{\partial R}{\partial T}\right)\Delta T = \kappa \Delta T$$

If the temperature calibration coefficient κ is known, ΔT can then be extracted from the measured ΔR. Thermoreflectance microscopy is a promising new means of mapping the thermal distribution of operating LEDs because it is a non-contact optical technique with very high spatial resolution (250nm) that is suitable for use on light emitting surfaces.

We have compared our thermoreflectance microscopy results to two more traditional means of estimating LEDs' temperature, based on temperature-induced variations in the emission wavelength and forward voltage of operating LEDs. Both of these techniques are bulk measurements that estimate a single temperature for the entire device, so they lack the ability to resolve thermal distributions across the LED surface. In addition, we compare thermal performance of encapsulated and de-encapsulated LEDs.

Our initial results from the wavelength shift measurement and forward bias voltage measurement show that the temperature of the encapsulated LED is lower than that of the de-encapsulated LED. This result suggests that silicone encapsulant and the lens act as a heat spreader and help conduct the heat from the active region of the LED device to the ambient. Compared these results with the thermoreflectance microscopy result, we find that the surface temperature is slightly higher than the p-n junction temperature, which is slightly higher than the

average operating temperature. Furthermore, the thermoreflectance microscopy provides the high resolution 2D temperature distribution across the LED surface which suggests that the temperature of the LED chip edge is higher than that of the center. Moreover, we obtain a 3-Dimensional temperature profile of the LED based on the three temperature measurement techniques.

Acknowledgements

First of all, I would like to thank my advisor, Janice Hudgings. This thesis would not have been possible without her guidance. I thank her for providing me with this wonderful and valuable research opportunity. Working in the lab has been the most important part of my undergraduate study. I have learned so much from the helpful discussions I had with her.

I would also like to thank Dr. Kadhair Al-hemyari for his incredible amount of time helping me in the lab. I appreciate all his comments, guidance, efforts and encouragement. Without his help, this research would not be possible. In addition, I would like to thank Joe Summers for all of his help when I first started the project and also his helpful and encouraging emails later.

Thank you, Prof. Rob Salgado and Prof. Dylan Shepardson, for being my thesis committee members.

The acknowledgement would not be complete without thanking many of the people who have supported me during this important time of my life. I would like to thank Len McEachern and Thomas Liimatainen for all their assistance in the setups, equipments, and computer issues. Thank you to all the labs members (Katie, Hexuan, Xiaolin, San, Amy, Sweta, Haibei and Joyce) for their help and encouragement. I am glad to have worked with you and it was an unforgettable experience.

Special thanks go to my dearest friends, especially Alen, who are always there, encouraging me, making me laugh and helping me throughout the year.

At the end, I would like to thank my parents, especially my mom, for their eternal understanding and love. Therefore, I would like to dedicate this thesis to them.

Sincerely,

Susu Yan

Mount Holyoke College

May 2, 2010

Table of Contents

1. Introduction

1.1 Motivation

A light-emitting diode (LED) is a semiconductor light source which converts electrical power to light. It has a long history, since electroluminescence was first discovered in 1907 using silicon carbide. The first creation of the LED is reported in 1962 as a practical electronic component [1]. Early LEDs emitted low-intensity red light. Over a half century's development, modern LEDs can generate different colors with wavelengths available across the visible, ultraviolet and infrared, and they have high brightness output light leading to a range of commercial applications.

The LED is based on the semiconductor diode which has a p-n junction structure. When forward bias voltage is applied to the diode, electrons can recombine with holes in the device and produce photons to generate light. This effect is called electroluminescence and the color of the output light is determined by the bandgap energy of the semiconductor material of the LED. The physics of the LED device will be explained in details in Chapter 2.

LEDs are used increasingly in daily life. They are used as indicators, such as the message displays in airports and railway stations. Many electronic devices use

LEDs, such as TVs and laptops. LEDs are also used in lighting and illumination, such as automotive lighting, street lights and architectural lighting.

Compared to traditional lighting systems, LEDs have many advantages. They are highly efficient lighting devices that produce more light per watt than incandescent bulbs. LEDs are compact, with a chip surface area of usually less than 1mm^2 [13], and the thickness of several hundred micrometers. They generate high brightness light but have low energy consumption compared to other lighting technologies. For example, an LED-based TV screen reduces the power consumption of TVs by 30%. LEDs also have a longer lifetime, usually around 30,000 hours which is equal to 25–30 years under normal use [13]. The lifetime for incandescent bulb is around 1,000 hours [13].

However, like light bulbs, LEDs generate a lot of heat, reaching temperatures of up to 45°C during normal operation [14]. The temperature affects the LED's performance, reliability, and lifetime. Therefore, there is a great deal of academic and industrial interests in how to conduct heat from an LED efficiently and how to accurately measure the temperature of the LED device. Thermal management and the operating temperature are critical in the LED design.

1.2 Prior Work on LED Temperature Measurement

Previously, researchers have used a variety of methods to study the temperature of LEDs. The infrared (IR) thermometry is the most widely used technique for temperature measurements. However the resolution for the IR method is above 1 mm [2], which is too coarse given the typical chip size of the LED. In addition, the IR measurement can only be used for a certain type of materials with limit refractive index range, which limits its use on LEDs. Moreover, an IR camera is expensive.

Thermocouple measurement, which is a direct method, is also difficult to apply for measuring the temperature of LEDs. Although this method is inexpensive and has 0.01 K thermal resolutions, it has no direct contact to the LED chip due to the silicone lens and silicone encapsulant around the LED chip. Thermocouple measurement is also hard to use on the light-emitting surface, and it can only measure the bulk temperature at a single point [5].

Wavelength shift measurement is a non-contact method of estimating the accurate p-n junction temperature of the LED. The peak wavelength of the emitted light is inversely proportional to the bandgap energy of the material of the LED. As the junction temperature increases, the bandgap energy decreases, and therefore increases the peak wavelength. Hence, by measuring the change in the

wavelength, accurate p-n junction temperature can be measured. Wavelength shift measurement is an attractive method. However, it is a bulk measurement that only estimates a single temperature of the entire device. In addition, wavelength shift measurement has poor resolution for measuring the peak wavelength of the LED. This is because the emitted light from the LED has a broad wavelength which makes it hard to determine where the peak is.

Forward bias voltage measurement is a commonly used indirect method of estimating the average temperature inside the LED. This method is measured across the entire device including contributions from the contact resistance as well as the junction voltage. Since both of these quantities are temperature dependent, forward bias voltage can be used to estimate an average operating temperature of the LED.

Previous works on the thermal management of the LED shows that the junction temperature and the ambient temperature affect the optical and electrical characteristics of LEDs, including the light output, electrical operating conditions and lifetime. Maintaining a lower junction temperature improves the light output of LEDs and results in a high reliability and a long life of the device. The junction temperature is affected by the power levels, heat sink, ambient temperature, etc [18].

1.3 Overview of My Work

Our goals in this project are: 1) measuring the thermal distribution inside the operating LED, both laterally and vertically in order to better understand the thermal performance of the LED; 2) apply a new technique of 2-Dimensional thermal mapping via thermoreflectance microscopy to obtain the first high resolution lateral temperature maps of the operating LED; 3) compare the results of the new thermoreflectance microscopy measurements with traditional methods of estimating the LED's temperature; 4) compare thermal performance of encapsulated and de-encapsulated LEDs.

In this project, we use two traditional methods which are described in the previous section, wavelength shift measurement and forward bias voltage measurement, as well as introducing a new method using thermoreflectance microscopy.

Thermoreflectance microscopy is a non-contact technique which can measure the 2-Dimensional temperature distribution across the operating LED surface. Unlike other methods, this technique has high spatial resolution (250nm) and high thermal resolution (10mK). Thermoreflectance microscopy measures the relative change in the reflectivity of a sample's surface as a function of a change in temperature [5]. Details of these three measurements will be discussed in

Chapter 2 and Chapter 3. Results of these measurements will be shown and discussed in Chapter 4. Conclusions will be discussed in Chapter 5.

2. Semiconductor Physics

A semiconductor material is the one that has conductivity between conductor and insulator. It has been increasingly used in the electronics industry. Many devices are made of semiconductors, such as solar cells, transistors, and light-emitting diodes. In semiconductor material, the current can be generated by free electron carriers or the free positive charged carriers, known as holes. The conductivity can be controlled by changing the chemical impurities and temperature, and by using illuminated light.

2.1 Energy Band Theory of Semiconductors

In solid-state materials, there are two main energy bands: valence band and conduction band, as shown in Figure 2.1.1. The valence band is defined as the highest energy band that contains electrons at absolute zero (T=0K). The valence band is occupied by localized electrons, and those electrons are not generally free to move in an electric field. The conduction band is the next highest energy band above the valence band. In Figure 2.1.1, the conduction band is separated from valence band and is positioned above the valence band for semiconductor and insulator. The insulator has a greater separation than the semiconductor. The conduction band and the valence band are overlapped for metal.

There is a bandgap, which has no electronic state existing within it, between the valence band and the conduction band. The energy of this bandgap is called the bandgap energy. Semiconductor materials usually have bandgap energy between 0.1 to 3eV [10].

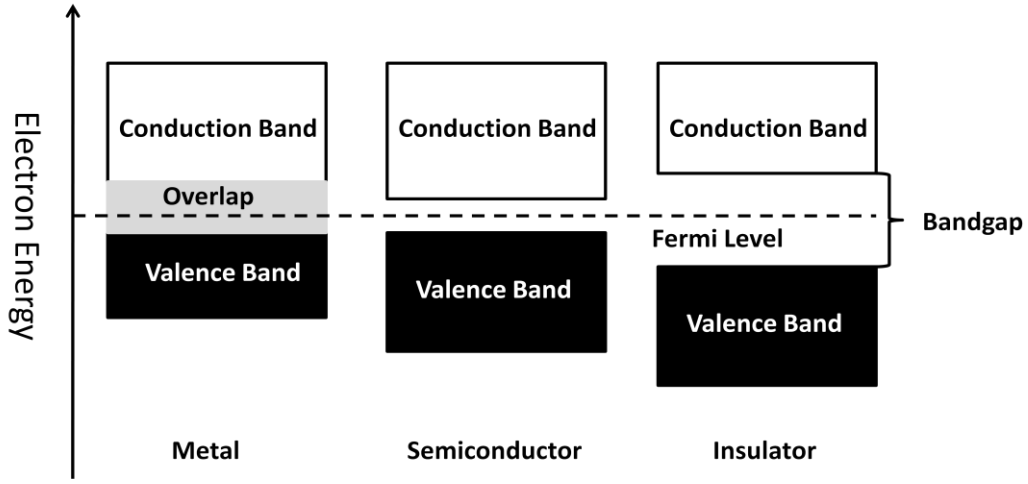

Figure 2.1.1: Energy band diagram for metal, semiconductor and insulator.

Electrons are most likely to occupy the lowest energy level first. Since the valence band has lower energy level than the conduction band, at absolute zero, the valence band is completely filled with electrons and conduction band is empty, as shown in Figure 2.1.2 (a). Therefore, there is zero conductivity, and no free charge carriers. A free charge carrier has electric charge and is mobile.

As the temperature increases, electrons can be thermally excited from valence to conduction band. The result is a partially empty valence band and a partially filled conduction band, as shown in Figure 2.1.2 (b). The unoccupied states left behind in the valence band are called holes. A hole carrier has a positive charge of +e. The electrons in the conduction band are mobile carriers, and each of them has negative charge of -e. Those electrons can drift to the holes in the valence band under the applied electrical field. Therefore, a drift current forms. The conductivity of the semiconductors increases sharply with increasing temperature because the amount of mobile carriers increases as electrons are thermally excited into conduction band.

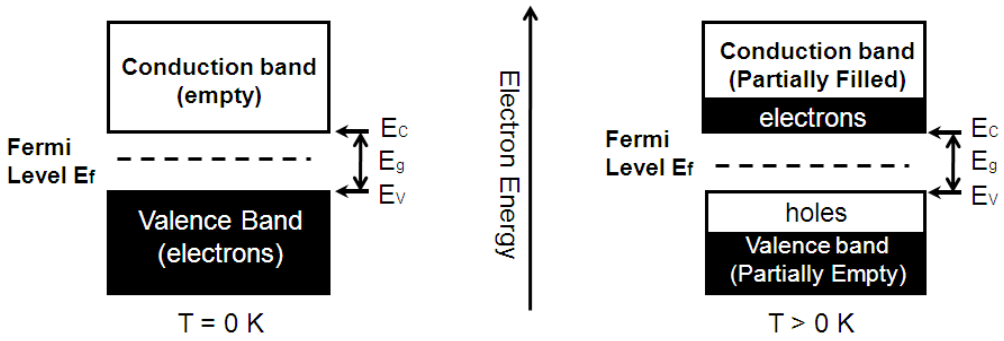

(a) **(b)**

Figure 2.1.2 (a): Energy band diagram for a semiconductor at absolute zero. (b): Energy band diagram for a semiconductor above absolute zero.

For an intrinsic semiconductor, which is a pure material without any chemical impurities, the concentration of electrons in the conduction band (n) equals the concentration of holes in the valence band (p), because those electrons and holes are from the thermal excitation and they are in pairs. One electron is excited from the valence band and leaves one hole in the valence band. By definition, $n = p = n_i$, where n_i is the intrinsic carrier concentration. It is the number of electrons in the conduction band or the number of holes in the valence band in intrinsic material. This number of carriers depends on the band gap of the material and on the temperature of the material. A large band gap makes it more difficult for an electron to be thermally excited across the band gap, and therefore the intrinsic carrier concentration is lower in higher band gap materials. Alternatively, increasing the temperature makes it more likely that an electron will be excited into the conduction band, which will increase the intrinsic carrier concentration.

Valence band energy (E_v) is the top level of valence band and the conduction band energy (E_c) is the bottom of conduction band, as shown in Figure 2.1.2. The bandgap energy is also defined as the difference between valence band energy and the conduction band energy:

$$E_g = E_c - E_v. \quad (2.1.1)$$

The Fermi level, also known as Fermi energy (E_f), is a very important parameter for semiconductors. It provides the probability $f(E)$ for an electron to occupy a certain state which has an energy E:

$$f(E) = \frac{1}{\exp\left[\frac{E-E_f}{k_B T}\right]+1} \quad , \tag{2.1.2}$$

where k_B is the Boltzmann constant and T is the absolute temperature. At absolute zero (T=0), if $E < E_f$, $f(E) = 1$, and if $E > E_f$, $f(E) = 0$. According to the previous explanation, since the valence band is completely occupied by electrons $f(E) = 1$ and the conduction band is empty $f(E) = 0$ at T=0, the Fermi level should be between the valence band and the conduction band, $E_V < E_f < E_C$. In addition, the Fermi level is also known as electronic chemical potential. In intrinsic semiconductor materials which are free from any impurities, the Fermi level is in the middle of the bandgap.

2.2 P-type and N-type Semiconductor

Besides increasing temperature, changing the concentration of impurities of the material can also increase the conductivity of a semiconductor because of the changing of mobile carriers' concentration. Impurity atoms, also known as dopants, are intentionally doped into the material during or after the crystal growth. Dopants that contribute electron carries are called donors. Dopants that

take away an electron from the semiconductor and leave the holes are called acceptors.

There are two types of semiconductors as shown in Figure 2.2.1 (a), (b). A p-type semiconductor is doped with acceptors which makes it contain more holes. The acceptor energy level occupies the energy E_A slightly above the valence band edge. The doped holes are easily created in the valence band; therefore the concentration of holes increases. In the p-type semiconductor, holes are the majority carriers while electrons are minority carriers. The Fermi level (E_f) moves down because the potential changes: there are more carriers in the valence band.

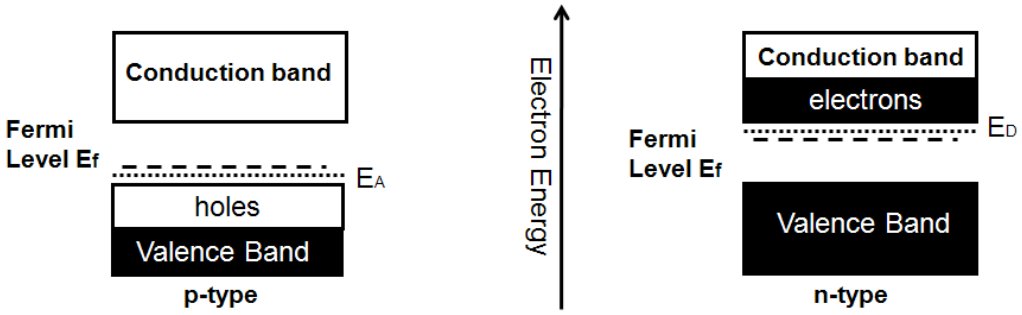

Figure 2.2.1 (a): n-type semiconductor energy band diagram. (b): p-type semiconductor energy band diagram.

An n-type semiconductor is doped with donors which makes it contain more electrons. The donor energy level occupies the energy E_D slightly below the

conduction band edge. The doped electrons are easily raised to the conduction band; therefore the concentration of electrons increases. In the n-type semiconductor, electrons are the majority carriers. On the contrary, holes are only formed through thermal excitation and are minority carriers. The Fermi level (E_f) moves up because the potential changes: there are more carriers in the conduction band.

In addition, the concentration of electrons and holes can be calculated under thermal equilibrium from the Fermi level:

$$n = n_i \exp[(E_f - E_i)/k_B T] \qquad (2.2.1(a))$$

$$p = n_i \exp[-(E_f - E_i)/k_B T] \ , \qquad (2.2.1(b))$$

where n_i is the intrinsic concentration, k_B is the Boltzmann constant, T is the absolute temperature, and E_i is the intrinsic Fermi level. Conversely, the Fermi level can be obtained when electrons or holes' concentration are known from Equation 2.2.1 (a), (b).

2.3 P-n junction

The p-n junction is when p-type and n-type semiconductors are physically brought in contact. The junction behaves very differently than either type of material separately. Current flows only in one direction, which is the forward bias,

but not in the other direction, which is the reverse bias. This characteristic creates the function of the basic diode.

Figure 2.3.1 (a) shows the diagram when p-type and n-type semiconductors are separated. Figure 2.3.1 (b) shows when p-type and n-type semiconductors are physically connected and form the p-n junction at thermal equilibrium [12]. The most important concept for p-n junction at thermal equilibrium is that the Fermi level is flat throughout the entire device structure. The Fermi level, also known as electronic chemical potential, is a function of temperature of the system. Temperature then is a measure of the internal energy of this system. At thermal equilibrium, there is no energy exchange between two subsystems which are the p-type and n-type semiconductor, so that the temperature is the same. Therefore, the Fermi level as a function of temperature is the same throughout the p-n junction.

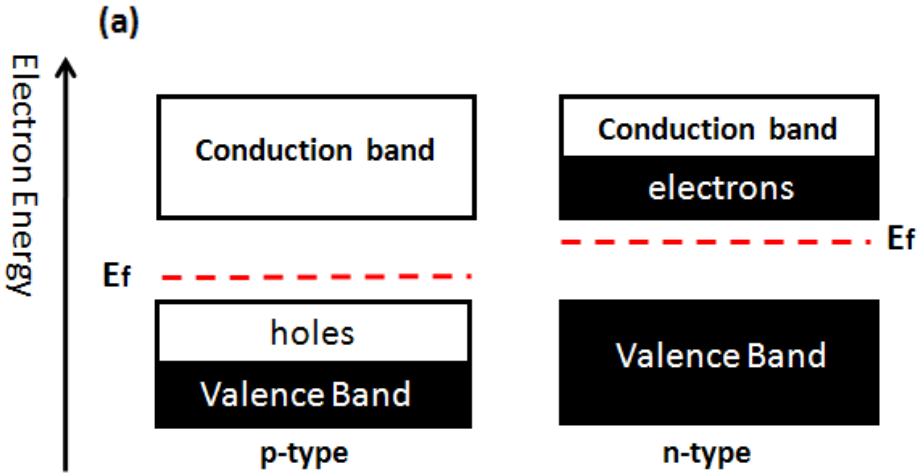

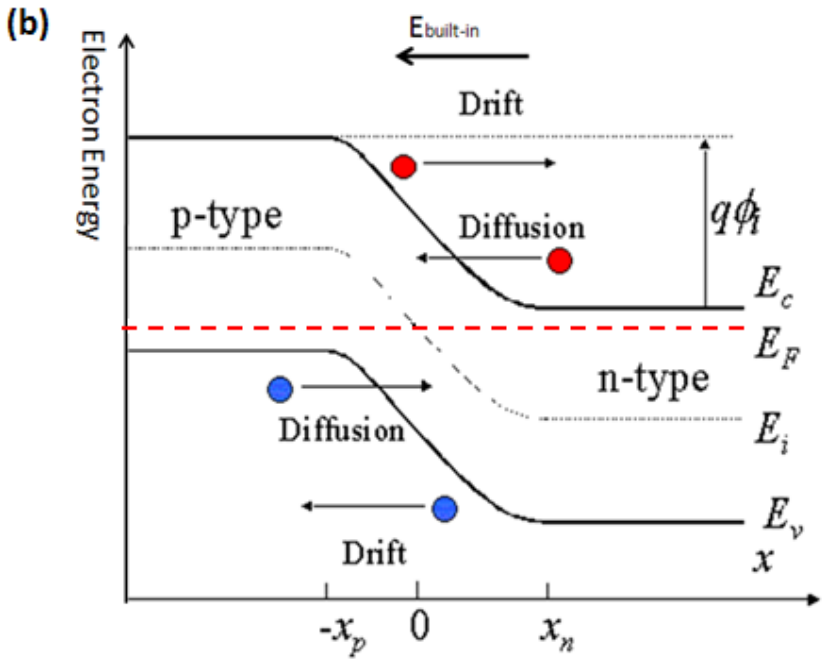

(b)

Figure 2.3.1 (a): p-type and n-type are separated. (b): p-type and n-type are connected and form p-n junction at thermal equilibrium [12].

As mentioned before, the p-type semiconductor is doped with holes and the n-type semiconductor is doped with electrons. The p-type has an excess of free holes compared to the n-type region, and the n-type has an excess of free electrons compared to the n-type. When p-type and n-type semiconductors are connected, electrons in the n-type semiconductor diffuse into p-type semiconductor with lower concentrations of electrons. Holes in the p-type semiconductor diffuse into the n-type semiconductor with lower concentrations of holes. Therefore, p-type has higher electron energy than n-type and a bend is formed from p-type to n-type. Fermi level, therefore, is aligned. Electrons recombine with the holes in p-type and leave positive charged ionized donors behind in the n-type semiconductor. Holes recombine with the electrons in n-type and leave negative charged ionized acceptors in the p-type semiconductor. This diffusion of electrons and holes causes diffusion current as well. Those ionized donors and acceptors are immobile and form a built-in electric field from n-type to p-type. In addition, this built-in electric field causes a drift of free carriers in the opposite direction: electrons in the p-type drift into n-type and holes in the n-type drift into p-type. The diffusion of carriers continues until the drift current balances the diffusion current, and therefore reaches thermal equilibrium.

A depletion region is formed at the p-n junction. This region is depleted of free charge carriers. The mobile charge carriers have diffused away by the built-in electric field. The only elements left in the depletion region are ionized donors and acceptors. Its width depends on the doping concentration.

The potential difference established across the junction caused by the built-in electric field is called the built-in potential, $q\Phi_i$. It is equal to the bending of the energy band:

$$q\Phi_i = E_g - E_{fp} - E_{fn} \ , \qquad (2.3.1)$$

where E_g is the bandgap energy, E_{fp} is the Fermi energy of p-type semiconductor and E_{fn} is the Fermi energy of n-type semiconductor.

When p-n junction is forward biased, which means a positive voltage is applied on p-type, there is an external electric field added in the opposite polarity to the built-in electric field, as shown in Figure 2.3.2 (a),. Therefore the potential difference between the two sides of the junction is lowered. The diffusion current greatly increases and the drift current decreases. This external electric field enhances the electrons and holes to recombine. A continuous recombination current is generated through the p-n junction from p-type to n-type. In the circuit in Figure 2.3.2 (b), there is a current (I) through the diode flowing in the opposite direction that the electrons are moving.

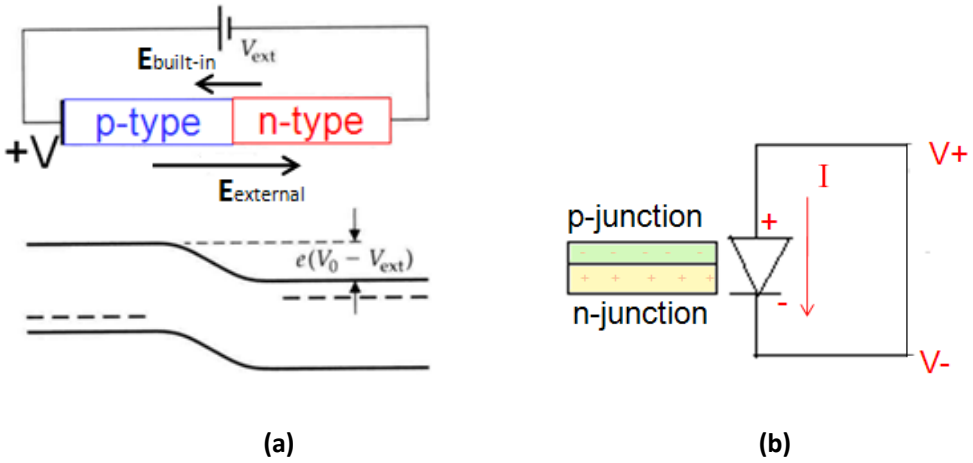

Figure 2.3.2 (a), (b): p-n junction is forward biased.

When p-n junction is reverse biased, which means we apply a negative voltage on p-type, there is an external electric field added in the same polarity to the built-in electric field, as shown in Figure 2.3.3 (a). Therefore the potential difference between the two sides of the junction is increased. This external electric field makes the depletion region continue to prevent further electrons and holes from recombining. The drift current increases due to the same polarity external electric field and the diffusion current decreases. When the reverse bias voltage is small, the drift current is slightly higher than the diffusion current. In the circuit shown in Figure 2.3.3 (b), there is almost no current flow.

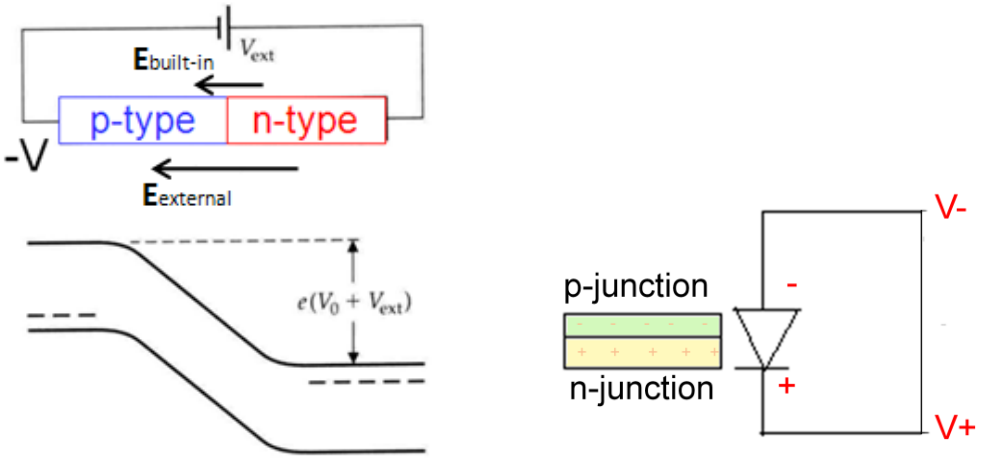

(a) (b)

Figure 2.3.3 (a), (b): p-n junction is reveres biased.

2.4 Light-emitting Diodes (LEDs)

2.4.1 LED Structure

Basic LED structure is shown in Figure 2.4.1. The top layer is p-type semiconductor and the n-type semiconductor is on the substrate. There is an active region where light is generated between the p-type and the n-type semiconductor. Electrons and holes recombination happens within this region. The active region usually consists of a single or multi quantum wells. The electrons from the conduction band and holes from the valence band are confined within the well. Therefore, the concentration of holes and electrons increases in

the quantum well active region. This is desirable for light emission (will be discussed in the next section).

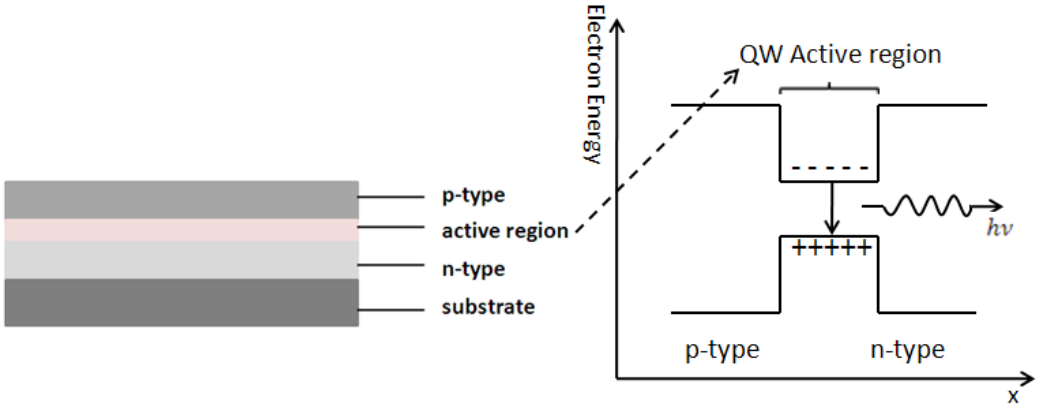

Figure 2.4.1: Basic light-emitting diode structure.

2.4.2 Electroluminescence

Spontaneous emission is when an electron spontaneously drops from an excited level to a lower level and emits a photon, as shown in Figure 2.4.2. As mentioned in section 2.1, thermal excitation can excite a few electrons from valence band to conduction band. The excited electron in the conduction band can spontaneously lose its energy and undergo a transition to the valence band, as shown in Figure 2.4.2. The electron recombines with the hole and the lost energy is emitted as a photon. This photon has energy equal to the bandgap energy:

$$E_g = h\nu. \tag{2.4.1}$$

where h is the Plank's Constant and ν is the frequency of the photon.

In LEDs, light is produced by spontaneous emission, referring to Figure 2.4.1.

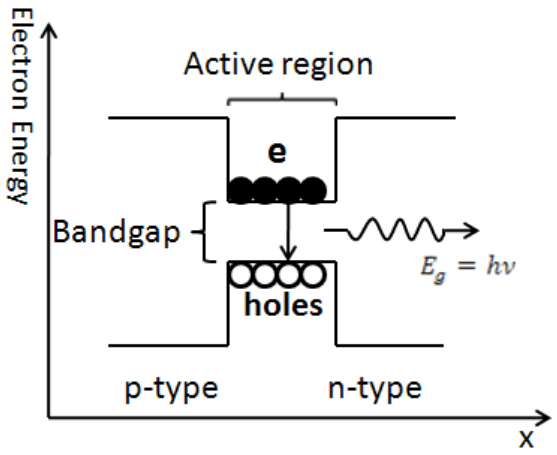

Figure 2.4.2: Spontaneous emission in the active region in the LED.

Electroluminescence, based on the spontaneous emission, is an optical and electrical phenomenon which means the material emits light when an electric current passes through it. It is the result of recombination of electrons and holes in the material. When forward voltage is applied, the active region captures the injected electrons and holes. The electrons spontaneously combine with holes and emit light continuously. The active region enhances the electroluminescence by capturing more electrons and holes, therefore, more light comes out.

2.4.3 Luxeon K2 Star Red LED Structure

Luxeon K2 Star Red LED is used in this project, as shown in Figure 2.4.3 [6]. This red LED is made of AlInGaP. The p-type and n-type semiconductor is made of Gallium Phosphide (GaP), and the active region is made of Aluminum Indium Gallium Phosphide (AlInGaP). P-type is positioned on the substrate and n-type is the top layer.

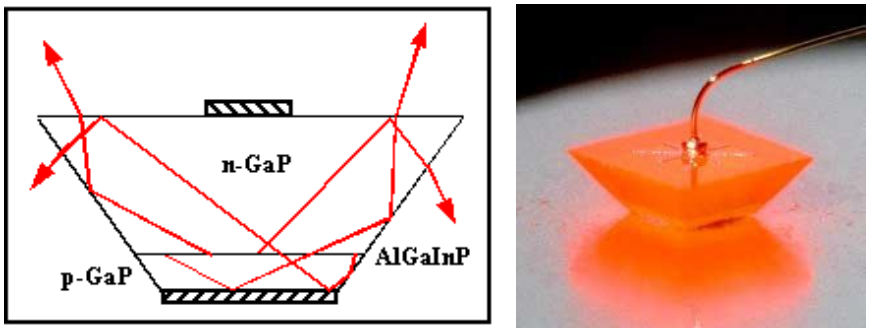

(a) **(b)**

Figure 2.4.3: Luxeon K2 Star Red LED structure.

The structure of the Luxeon K2 Star Red LED chip is a Truncated Inverted Pyramid (TIP) configuration, as shown in Figure 2.4.3 (a) [6]. The TIP geometry improves light extraction by redirecting many of the internally reflected photons from the sidewall interfaces towards the top surface of the chip, allowing them to

escape. Therefore, the amount of output light is increased. Figure 2.4.3 (b) shows when the red light is emitted from the LED.

2.4.4 Characteristics

Figure 2.4.4 is a current-voltage (IV) curve for LED [7]. There are three regions: the breakdown region is when a great reverse voltage is applied, and LED may be damaged (referring to Figure 2.3.3); the reverse region is when a reasonable reverse voltage is applied, and there is little reverse current flowing from negative terminal to positive terminal (referring to Figure 2.3.3); the forward region has a turn-on voltage under which there is little current, and as the forward bias voltage increases, the current greatly increases (referring to Figure 2.3.2). Experimental results will be shown and discussed in Chapter 4.

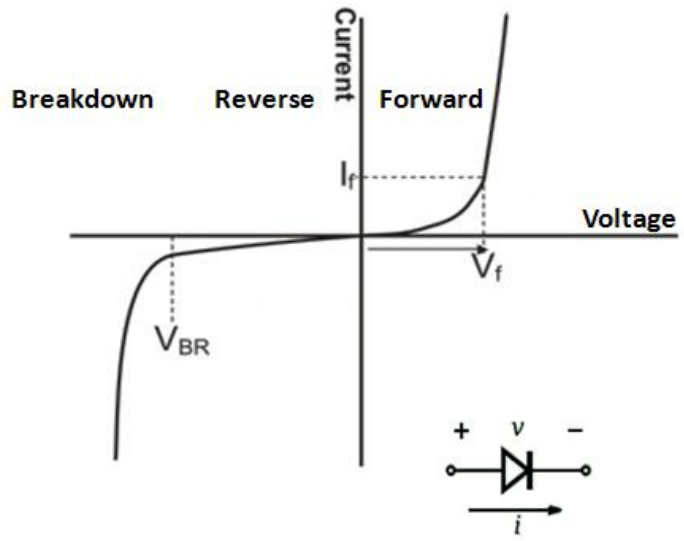

Figure 2.4.4: LED current-voltage (IV) curve [7].

LED's wavelength is another important characteristic. The wavelength for the same LED device can shift to the right with increasing current and temperature, as shown in Figure 2.4.5. This shift is also known as red shift which suggests that the color changes from blue to red. Therefore, a change in temperature can cause the change in output light color. For each material, there is an expansion coefficient. When the material is heated, the coefficient increases and the atoms in the material will be further away so that there is less overlapping between them. Since the band gap energy is the energy needed to break a bond in the crystal. When a bond is broken, the electron has absorbed enough energy to leave the valence band and drop to the conduction band and undergoes the spontaneous emission. Less overlapping between atoms decreases the bandgap

energy. Equation 2.4.2 shows the relationship between the wavelength and the bandgap energy:

$$\lambda_g = \frac{hc}{E_g} \ . \qquad (2.4.2)$$

where c is the speed of light. From equation 2.4.2, when the bandgap energy decreases, the wavelength increases. Experimental results will be shown and discussed in Chapter 4.

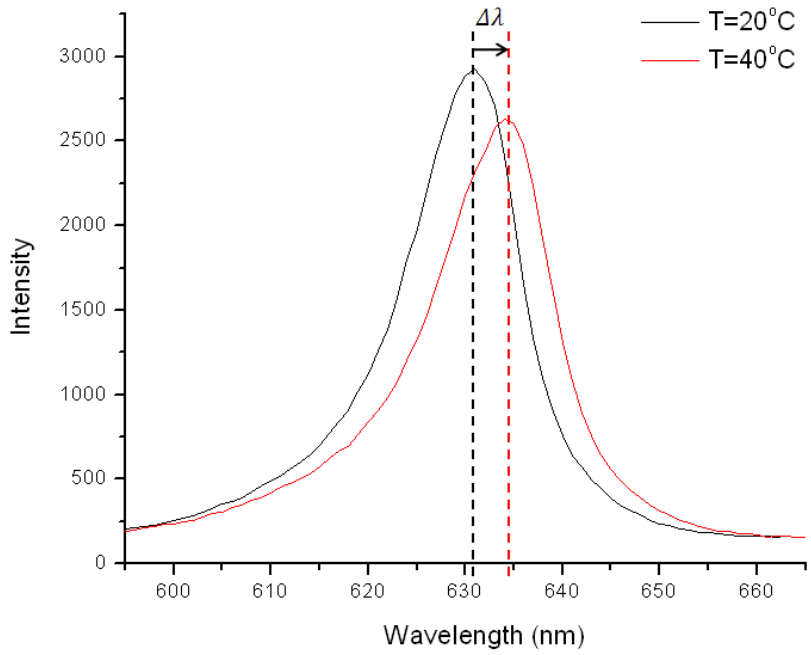

Figure 2.4.5: LED wavelength is redshifted.

The accurate junction temperature can be obtained from the wavelength shift measurement. According to Figure 2.4.2 and the discussion in section 2.4.2, the

light is generated from the active region, which is located at the p-n junction. The wavelength of the output light can be measured. In addition, the change in the peak wavelength depends on the change in the temperature as discussed in the previous paragraph. Therefore, by measuring the wavelength shift, the active region temperature can be obtained [4].

2.4.5 Temperature of the LED

There are mainly three different temperatures on the LED: the p-n junction temperature, the surface temperature and the average temperature across the device, Figure 2.4.6.

The p-n junction temperature is due to the heat which is generated from the active region at the p-n junction. When forward voltage is applied to LED, the external electrical field causes the electrons and holes recombination in the active region. Some of the injected electrical power is converted to light. The rest of the power is converted to heat due to the non-radiative recombination. Therefore, heat is generated from the active region. The p-n junction temperature can be calculated by measuring the wavelength shift which is discussed in the previous section.

The heat which is generated from the active region is transferred to the top

and the bottom of the LED. The surface temperature is related to the reflectivity of the surface and can be calculated from the thermoreflectance microscopy. Details will be discussed in Chapter 3.

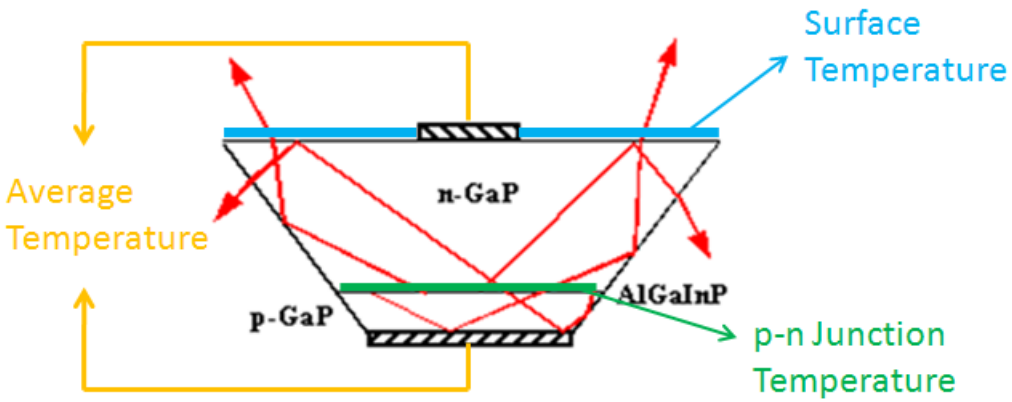

Figure 2.4.6: Different temperature of the Luxeon K2 Star Red LED.

The average operating temperature across the LED can be calculated by measuring the forward bias voltage. When the forward voltage is added to the device, the LED can be considered as a temperature dependent variable resistor, as shown in Figure 2.4.7 (a), (b). As the temperature increases, more dopants in the p-type and n-type semiconductor are ionized. Therefore, the conductivity of the p-n junction increases and the resistance decreases. Based on the Ohm's law, at same injected current, the voltage decreases as the resistance decreases. Thus, by measuring the change in the forward voltage, the average temperature across

the p-n junction can be calculated. More details will be discussed in Chapter 3.

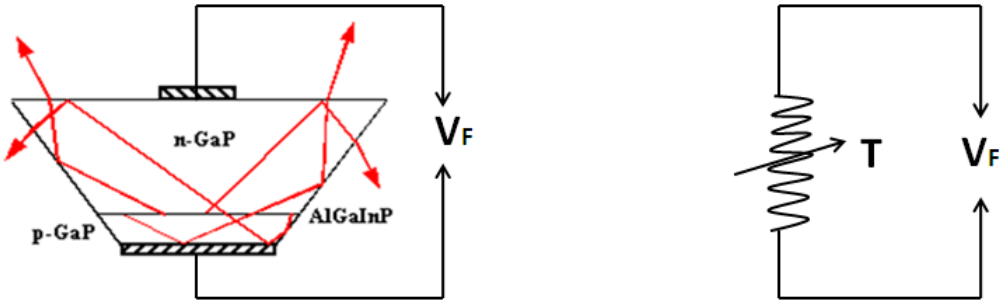

(a) **(b)**

Figure 2.4.7 (a): Forward bias voltage is applied to the LED device. (b): Equivalent stricture of the LED device—a temperature dependent variable resistor.

2.4.6 Packaging

Figure 2.4.8 shows the overall packaging construction of the AlInGaP Luxeon K2 Star Red LED [8]. The LED chip is mounted on the metal thermal heatsink slug, which is made of high thermal conductivity material. The heatsink slug provides a high efficiency thermal path to extract heat from the active region of the LED to the packaging. The LED chip is connected to anode and cathode leads by the bond wire. The LED package has a soft silicone lens on the top. The space between the LED chip and the lens is filled with a silicone encapsulant. The silicone materials are a good thermal management material which can endure high temperature, transfer heat from components to the environment, are electrical

insulated, and are flexible to fix in the space and to protect the components [9, 13]. Therefore, the silicone lens and the silicone encapsulant in the Luxeon K2 Star Red LED package protect the LED chip and conduct heat, which is generated from both the LED surface and the junction, to the environment. Experimental results will be shown and discussed in Chapter 4.

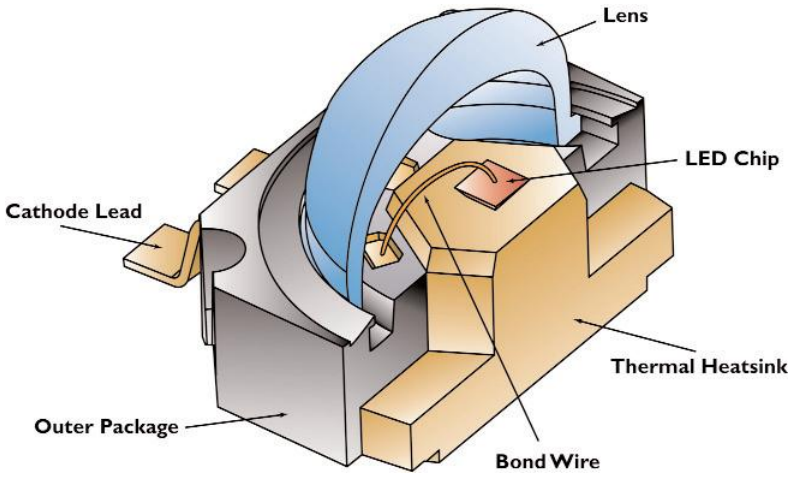

Figure 2.4.8: Overall packaging construction of AlInGaP Luxeon K2 Star Red LED [8].

Figure 2.4.9 shows the internal construction of the AlInGaP Luxeon K2 star LED package [8]. The Truncated Inverted Pyramid (TIP) LED chip is bonded to the thermal heatsink slug. The LED chip and the heatsink slug are connected to the anode and cathode pins using gold wires.

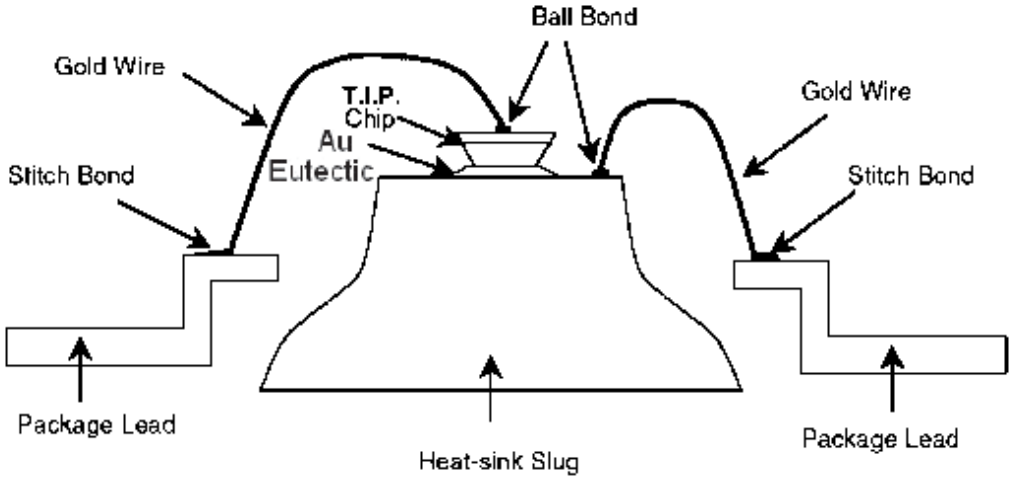

Figure 2.4.9: Internal construction of Luxeon K2 Star Red LED [8].

3. Methods (Experimental setups)

In this chapter, the experimental setups used in project are explained. In the beginning, the basic characterization of the Luxeon K2 Star Red LED is performed: the current-voltage (IV) curve, optical power-current (LI) curve and the spectrum. As mentioned in the previous chapter, three measures of temperature are performed to study three different temperatures of the LED. The wavelength shift measurement is conducted to measure the p-n junction temperature. The forward voltage measurement is performed to measure the average temperature across the LED device. Finally, thermoreflectance microscopy is used to measure the 2D temperature distribution across the LED surface.

3.1 De-encapsulation Procedure

We use two types of LEDs in the project: the encapsulated and de-encapsulated LED, as shown in Figure 3.1.1 (a), (b). For the de-encapsulated LED, we use a blade to take off the silicone lens and most of the silicone encapsulant. Then we add one drop of silicone solvent (Dynasolve) to the LED chip and put it on the hot plate (Barnstead Super Nuova) at 70℃ for 5 minutes,

and we repeat this step until all the silicone encapsulant are dissolved. After rinsing the LED in the isopropanol, we use the ultrasonic cleaner to clean it; therefore the de-encapsulated LED is obtained.

(a) 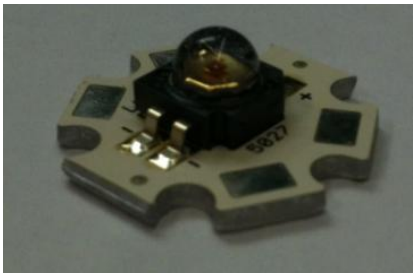 **(b)** 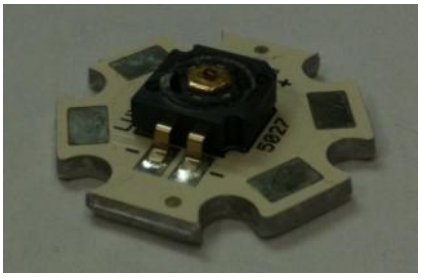

Figure 3.1.1: (a) Encapsulated Luxeon K2 Star Red LED. (b) de-encapsulated Luxeon K2 Star Red LED.

3.2 Basic Characterization

In order to measure the basic characteristics such as current voltage (IV) and optical power-current (LI) curves of the encapsulated and de-encapsulated LEDs, we constructed the experimental setup as shown in Figure 3.2.1.

The LED under test is mounted on a Thorlabs mount (TCLDM9 Model) with an integrated thermoelectric cooler (TE cooler) attached beneath the test device. The temperature controller is used to control the TE cooler, which determines the case temperature of the LED. The current source (ILX Lightwave LDX 3232 Precision Laser Diode Current Source) is connected to the LED and used to apply current to it. In order to collect as much emitted light as possible for accurate measurement, we inserted the LED and a large area silicon photodetector inside

an integrating sphere. The photodetector is then connected to a power supply (Hewlett-Packard; E3620A Dual Output Power Supply), which is in series with a digital multimeter (Keithley 197A Autoranging Microvolt Digital MultiMeter). The power supply applies a bias voltage to the photodetector and the digital multimeter is used to measure the photodetector current. By connecting the digital multimeter and the current source to the computer via a GPIB connection, the LED drive current is set by a LabVIEW program while the LED forward voltage and the photodetector current are read by the same LabVIEW program. The current-voltage (IV) curve data is then plotted using the software package Origin.

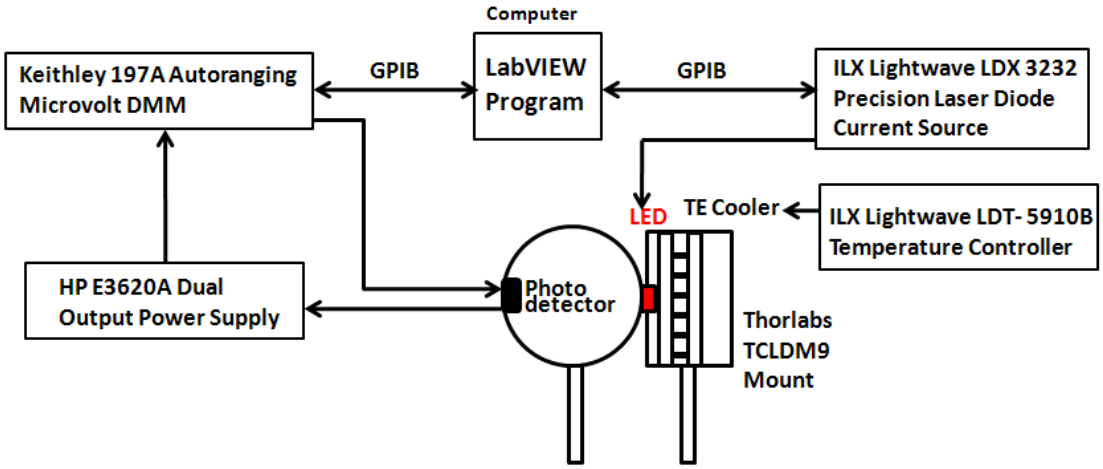

Figure 3.2.1: IV and LI curve measurement setup.

In order to calibrate photodetector current to optical power, the photodetector and the sphere are replaced by an optical power head (ILX Lightwave OMH-6703B Silicon Power Head), which is connected to an optical multimeter

(ILX Lightwave OMM 6810B Optical Multimeter) as shown in Figure 3.2.2. The optical power is read from the optical multimeter which allows us to determine the relationship between optical power and the LED drive current.

Based on the relationship between photodetector current and the LED drive current, which is obtained from the setup in Figure 3.2.1, and the relationship between optical power and the LED drive current, which is obtained from the setup in Figure 3.2.2, the photodetector current can be converted to optical power. Therefore the optical power-current (LI) curve can be obtained. IV and LI results will be shown and discussed in Chapter 4.

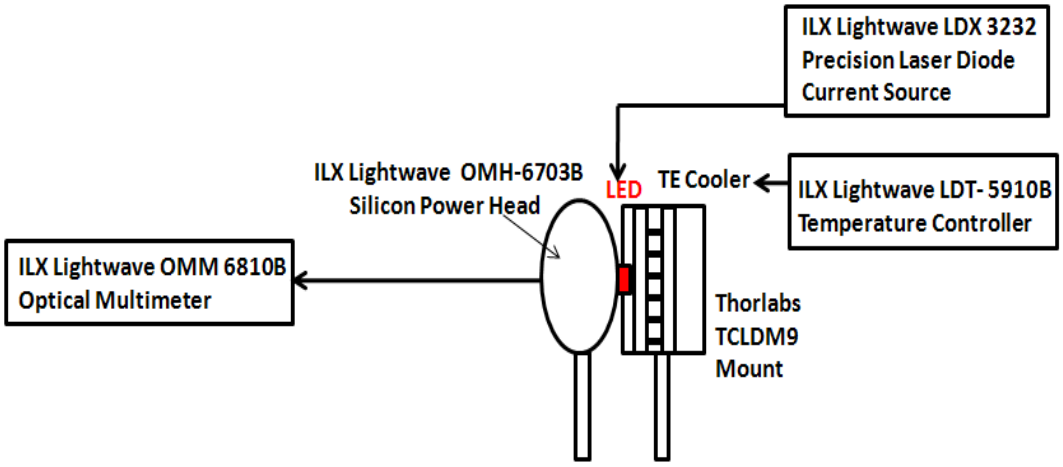

Figure 3.2.2: Calibrate photodetector current to optical power.

3.3 Spectrum and Peak Wavelength Shift Measurement

Figure 3.3.1 shows the setup for measuring the spectrum and the wavelength shift for the encapsulated and de-encapsulated LED. The LED, the mount, the TE

cooler and the current source in this setup are the same as they are used in the previous setup.

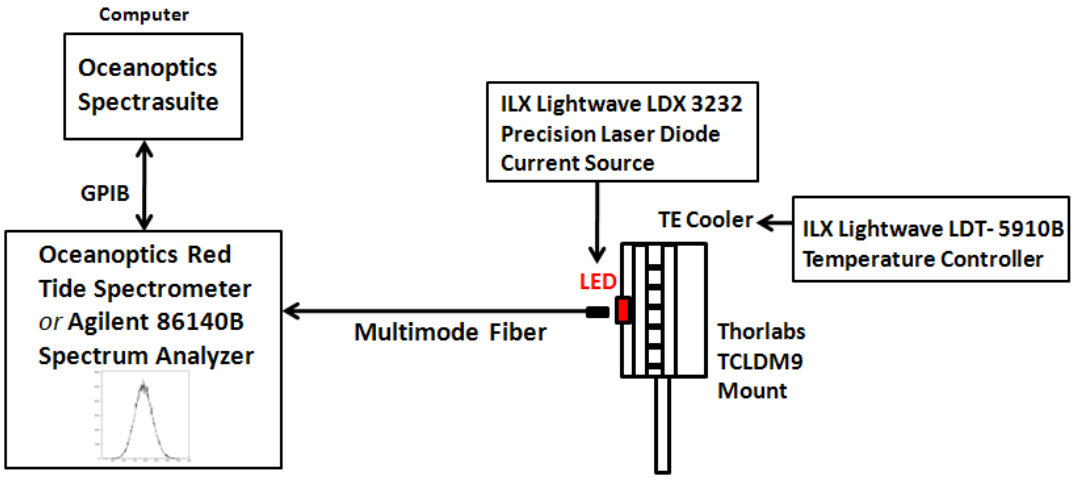

Figure 3.3.1: Spectrum and wavelength shift measurement.

To measure the spectrum, a multimode fiber (50μm core) is connected to a spectrometer (Oceanoptics Red Tide Spectrometer), and the end facet of the fiber is held on a three dimension translational stage and placed close to the output facet of the LED, as shown in Figure 3.3.1. The spectrum of the LED is obtained by a computer which is connected to the spectrometer with GPIB connection. By using the Spectrasuite software (Oceanoptics), the data can be exported to Origin and plotted.

In order to improve the accuracy, we use the spectrum analyzer (Agilent 86140B Optical Spectrum Analyzer) in place of the spectrometer to measure the peak wavelength of the LED, as shown in Figure 3.3.1. Different case

temperatures can be set by the temperature controller and the drive current can be changed by the current source. The peak wavelength and the corresponding injected current and case temperature are recorded and plotted in Origin. Results will be shown and discussed in Chapter 4.

3.4 Forward Voltage Measurement

The forward voltage measurement consists of two steps: 1) the case temperature and the forward voltage of the LED are calibrated in order to obtain the calibration coefficient α; 2) the experimental average operating temperature is measured while applying a pulsed current.

Figure 3.4.1 shows the experimental setup for the calibration which is used to obtain the calibration coefficient α. The current source (ILX Lightwave LDX 3220 Precision Laser Diode Current Source) is used to drive the LED with a low measurement current in order to reduce the self-heating at the p-n junction. Therefore, in steady state, the TE cooler temperature (case temperature), which is controlled by the temperature controller, can be assumed as the average operating temperature [3]. A T-type thermocouple (Sable Systems TC1000 thermocouple meter) is used to separately measure the case temperature. By using the four-wire technique, the accurate forward biased voltage (V_f) across the LED is measured by

a multimeter (Keithley 175A Autoranging Multimeter). By plotting the voltage and the temperature in Origin, calibration coefficient α is obtained:

$$\Delta V_f = \alpha \Delta T. \quad (3.4.1)$$

A multimeter (Keithley 197A Autoranging Microvolt DMM) is used to read the drive current, and another multimeter (Keithley 175A Autoranging Multimeter) is used to read the voltage across the LED, therefore calculating the injected electrical power. The calibration results will be shown and discussed in Chapter 4.

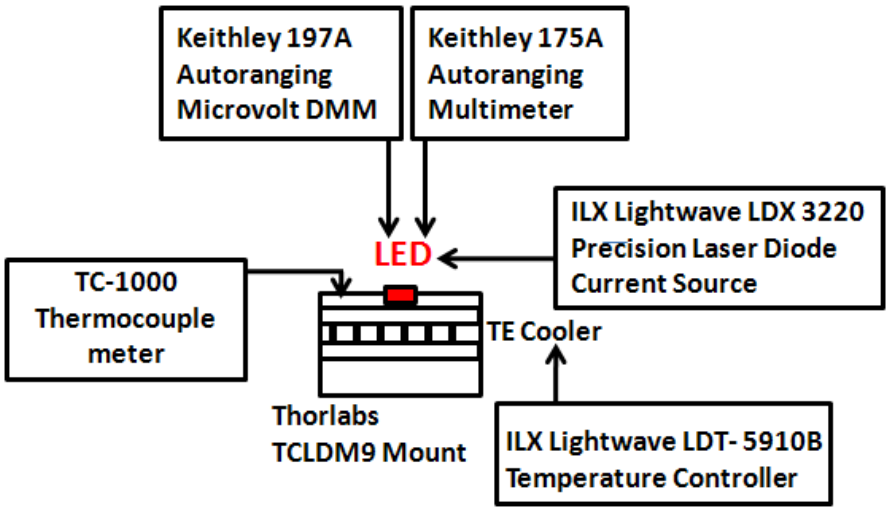

Figure 3.4.1: Forward bias voltage measurement calibration setup.

A pulsed current measurement is then performed by using the setup shown in Figure 3.4.2. In Figure 3.4.3, we show an illustration of the applied pulsed current. A function generator (Agilent 33220A 20MHz Function/Arbitrary Waveform

Generator) is used to apply a pulsed current to the LED through the current source. A high operating current is applied to the LED for a long period of time and then quickly turned down to a low measurement current. The high current simulates the normal operating conditions, and heats the sample. On the other hand, the low current is the same value as the one we used in obtaining the calibration coefficient. This pulsed current allows us to determine the change in the biased voltage due to the self-heating of the LED. The duty cycle, which is the pulse duration divided by the pulse period, is set at a very small value (0.02%) to ensure that the LED is heated up in a normal operation at a high current typically, and will not have sufficient time to be cooled down at a low measurement current (typically around a few milliamps). The period is set at a reasonably high value which also ensures that the high operating current is applied long enough to heat the LED.

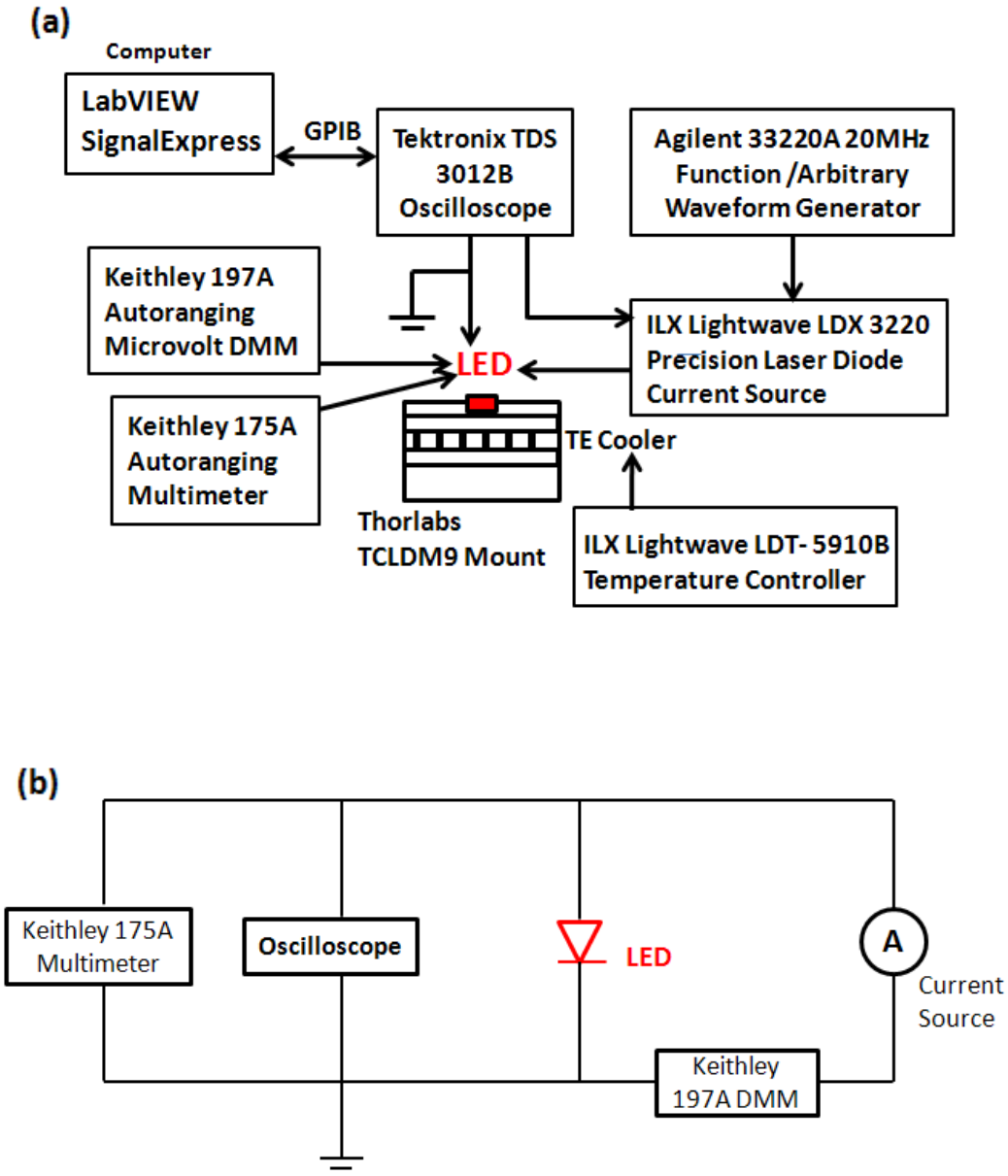

Figure 3.4.2: (a) Pulsed current measurement. (b) Equivalent circuit.

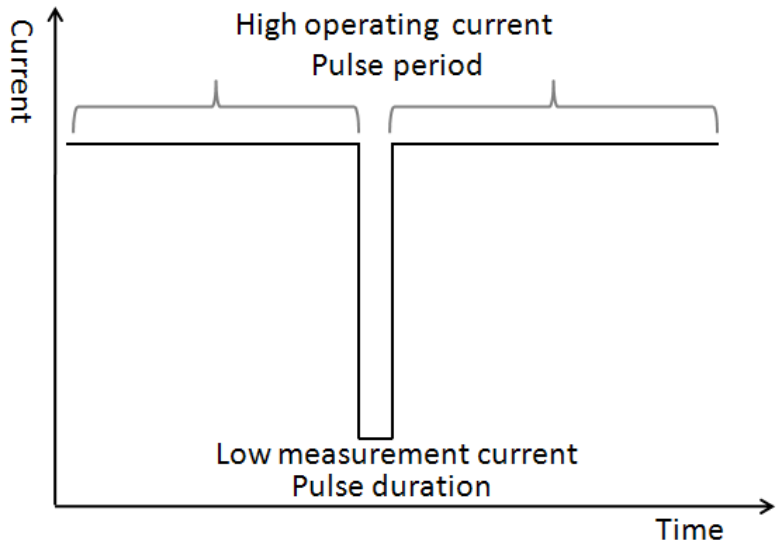

Figure 3.4.3: Schematic of the applied pulsed current.

In order to measure the pulsed voltage, the oscilloscope (Tektronix TDS 3012B Oscilloscope) is connected to the current source and the LED. By using the NI LabVIEW SignalExpress Tektronix Edition software on a computer which is connected to the oscilloscope with a GPIB connection, the pulsed voltage graph is obtained. Data can then be exported to Origin and plotted.

Figure 3.4.4 shows the explanation of measuring the change in the forward voltage (V_f). A reference voltage (black curve) is obtained by applying a DC signal with low measurement current. The off-state forward voltage corresponding to different applied maximum currents can be measured on the graph, for example: the pink curve it the off-state forward voltage with 469.94mA

applied maximum current. The change in the forward biased voltage is obtained by comparing the off-state forward voltage with the reference voltage. Two multimeters are used to record the applied maximum current and the associated voltage. They are also used to ensure that the off-state current is the same value as the current used in the calibration.

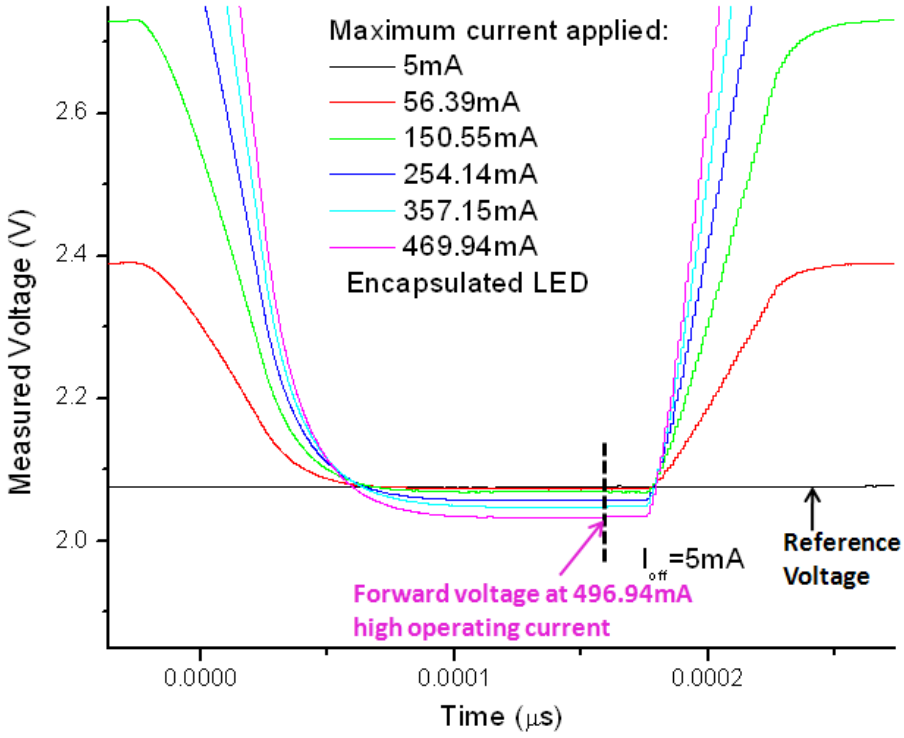

Figure 3.4.4: Explanation of measuring the change in the forward voltage.

The change in temperature (ΔT) then can be calculated from Equation 3.4.2, with the change in forward voltage resulting from the previous calculation and the

corresponding calibration coefficient α resulting from the calibration. The average operating temperature, therefore, is obtained by adding ΔT and the case temperature:

$$T = T_{case} + \Delta T. \tag{3.4.2}$$

3.5 Thermoreflectance Microscopy

In the third part of our experimental measurement of the temperature of the LED, we use a method called thermoreflectance microscopy. It is a non-contact, optical method which can be used to measure the 2D temperature distribution of the LEDs' surface. The basic theory is that the reflectivity (R) of the LED surface is a function of the surface temperature (T).

The refractive index (n) of a material changes when the temperature of the material is modulated. The reflectivity (R) of a material depends on its refractive index:

$$R = \left(\frac{n-1}{n+1}\right)^2 \tag{3.5.1}$$

Therefore, a change in the temperature (ΔT) of a material causes a change in its reflectivity (ΔR). For a small change in ΔT, we can approximate ΔR by:

$$\Delta R = \frac{\partial R}{\partial T}\Delta T. \tag{3.5.2}$$

Dividing R on both sides of the equation leads to the common thermoreflectance equation:

$$\frac{\Delta R}{R} = \left(\frac{1}{R}\frac{\partial R}{\partial T}\right)\Delta T = \kappa \Delta T \qquad (3.5.3)$$

where κ is a material dependent temperature calibration coefficient.

In our project, we measure $\frac{\Delta R}{R}$ experimentally, as shown above. For the AlGaInP LED used in this project, we take $\kappa = 8 \times 10^{-5}$ (K^{-1}). This value was determined experimentally by a prior researcher [9].

The experimental setup for the thermoreflectance measurement is shown in Figure 3.5.1 (a). A CCD camera (Opteon 25194 CCD Camera; 60 frames/second; 652x494 pixels) and standard optical microscope are used to generate a 2D map of $\frac{\Delta R}{R}$ across an operating LED surface in response to an applied temperature modulation (ΔT).

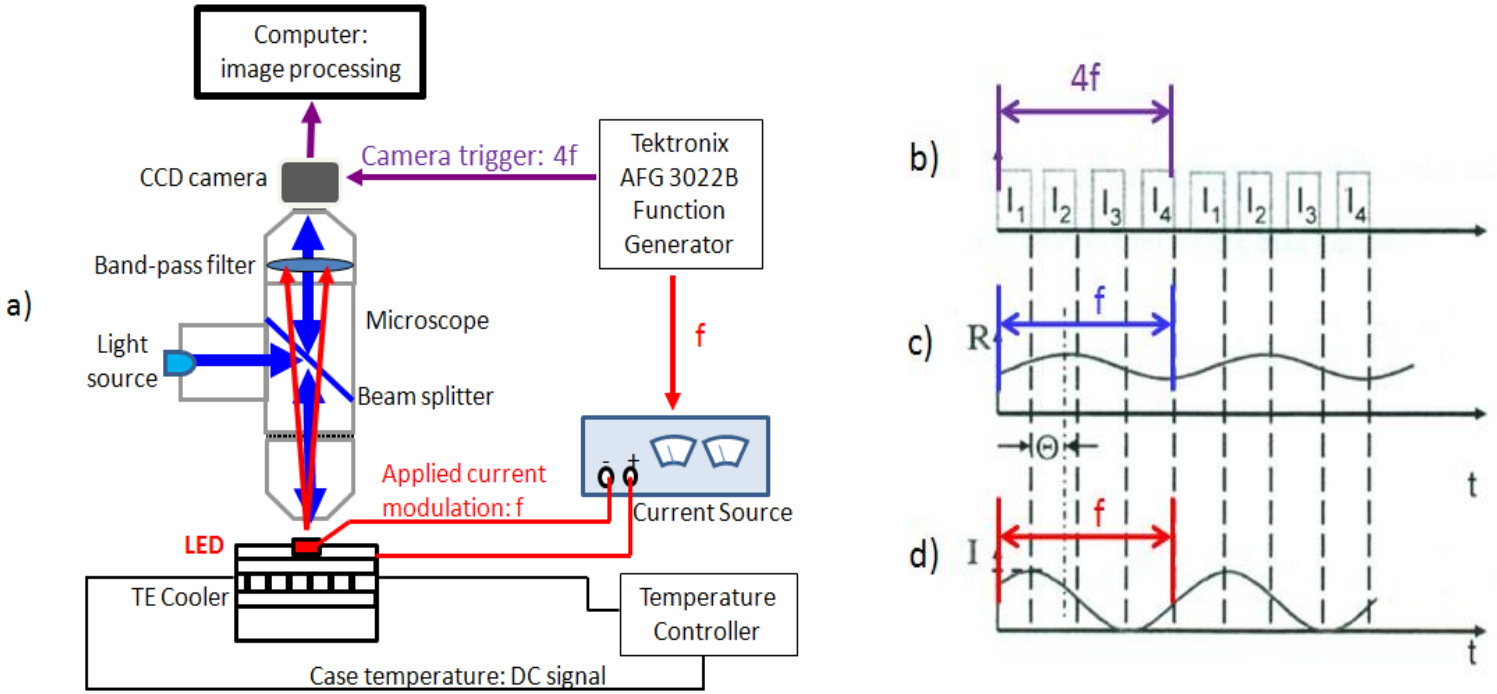

Figure 3.5.1: a) Thermoreflectance microscopy setup. b) CCD trigger TTL signal with frequency of 4f. c) Blue light source reflected signal with frequency of f. d) LED being tested with modulated drive current at frequency f.

The LED, the mount, the TE cooler, the temperature controller and the current source are the same as in the previous setup. The light source is a blue LED with 470nm peak wavelength. The blue LED light illuminates the surface of the red LED under test and is reflected off the surface of the red LED. The reflected light is transmitted upwards through the microscope to illuminate the CCD camera. A bandpass filter (Chroma Technology D470/20x) is used to block the emitted light from the red LED (~635nm), while allowing the reflected blue LED light (470nm) to be detected by the CCD camera.

Because the relative change in reflectivity ($\frac{\Delta R}{R}$) in response to a temperature modulation (ΔT) is small (typically ~10^{-4}), a lock-in integration measurement technique must be used. In our work, we use a "four-bucket" signal processing technique to effectively perform pixel by pixel lock-in amplification, independently locking each individual pixel of the CCD camera to the temperature modulation frequency f. By using this technique, we measure $\frac{\Delta R}{R}$ at each pixel of the camera. Therefore, this measurement enables us to construct a 2D map of $\frac{\Delta R}{R}$ across the test device surface, from which a 2D thermal map can be extracted by knowing κ. The lock-in technique is implemented as follows.

A function generator (Tektronix AFG 3022B Dual Channel Arbitrary Function Generator) is connected to the current source to modulate the red LED with a sinusoidal current at frequency f, as shown in Figure 3.5.1 (d). Hence, the temperature of the red LED then is modulated primarily at frequency f as well.

Since the change in reflectivity is a function of the changing temperature, the blue LED reflected signal is also modulated primarily at frequency f by the red LED's modulated temperature, as shown in Figure 3.5.1 (c). The CCD camera is triggered by the other channel of the function generator with a TTL signal at a frequency which is 4 times the red LED modulated frequency, as shown in Figure 3.5.1 (b). The LED and camera signals are phase-locked. In this project, the LED modulated frequency is 10Hz, and the camera is triggered at 40Hz.

The modulated reflectivity R, which is time (t) and position (x, y) dependent, with frequency of f is depicted in Equation 3.5.4:

$$R(x,y,t) = R_0(x,y,t) + \Delta R(x,y,t)\cos(2\pi ft + \varphi(x,y) + \Psi) \ . \qquad (3.5.4)$$

R_0 is the average reflectivity at a given point and given time. ΔR is the reflectivity modulation amplitude. $\varphi(x,y)$ is the phase shift between the injected modulated current and the resulting modulated temperature. Ψ is an additional the phase shift resulting from experimental consideration, such as delay in the electronics. With a camera trigger frequency of 4f, the camera takes four images during each period T=1/f. The integration time for each image is set to T/4 multiply by 97%, which we approximate as T/4 below. Each pixel of each image has its corresponding intensity which can be calculated by integrating over the optical intensity collected at each pixel:

$$I_1 = \int_0^{\frac{T}{4}} R(x,y,t)\,dt \qquad I_2 = \int_{\frac{T}{4}}^{\frac{T}{2}} R(x,y,t)\,dt$$

$$I_3 = \int_{T/2}^{3T/4} R(x,y,t)\,dt \qquad I_4 = \int_{3T/4}^{T} R(x,y,t)\,dt \ . \qquad (3.5.5)$$

By plugging in the reflectivity equation into the above integration, we get:

$$\mathrm{I}_1 = \frac{T}{4}\mathrm{R}_0 + \frac{\mathrm{T}}{2\pi}\Delta\mathrm{R}[\cos(\varphi + \Psi) - \sin(\varphi + \Psi)]$$

$$\mathrm{I}_2 = \frac{T}{4}\mathrm{R}_0 + \frac{\mathrm{T}}{2\pi}\Delta\mathrm{R}[-\sin(\varphi + \Psi) - \cos(\varphi + \Psi)]$$

$$\mathrm{I}_3 = \frac{T}{4}\mathrm{R}_0 + \frac{\mathrm{T}}{2\pi}\Delta\mathrm{R}[-\cos(\varphi + \Psi) + \sin(\varphi + \Psi)]$$

$$\mathrm{I}_4 = \frac{T}{4}\mathrm{R}_0 + \frac{\mathrm{T}}{2\pi}\Delta\mathrm{R}[\sin(\varphi + \Psi) + \cos(\varphi + \Psi)] \qquad (3.5.6)$$

Hence the intensities $(\mathrm{I}_1 - \mathrm{I}_4)$ measured at each pixel can be used to extract DC signal R_0 (Eq. 3.5.7), AC signal $\Delta\mathrm{R}$ (Eq. 3.5.8), phase signal $\varphi(\mathrm{x},\mathrm{y}) + \Psi$ (Eq. 3.5.9), and AC/DC signal $\Delta\mathrm{R}/\mathrm{R}_0$ (Eq. 3.5.10):

$$\mathrm{R}_0(\mathrm{x},\mathrm{y},\mathrm{t}) = \frac{(I_1+I_2+I_3+I_4)}{T} \qquad (3.5.7)$$

$$\Delta\mathrm{R}(\mathrm{x},\mathrm{y},\mathrm{t}) = \frac{\pi}{\sqrt{2}T}[(I_4 - I_2)^2 + (I_1 - I_3)^2]^{1/2} \qquad (3.5.8)$$

$$\varphi(\mathrm{x},\mathrm{y}) + \Psi = \tan^{-1}\frac{I_1+I_2-I_3-I_4}{I_1-I_2-I_3+I_4} \qquad (3.5.9)$$

$$\frac{\Delta\mathrm{R}(\mathrm{x},\mathrm{y},\mathrm{t})}{\mathrm{R}_0(\mathrm{x},\mathrm{y},\mathrm{t})} = \frac{\pi}{\sqrt{2}}\frac{[(I_4-I_2)^2+(I_1-I_3)^2]^{1/2}}{I_1+I_2+I_3+I_4} \quad . \qquad (3.5.10)$$

Thus, if there were no noise in the experiment, we could calculate 2D maps of the amplitude $(\frac{\Delta\mathrm{R}}{\mathrm{R}} = \kappa\Delta\mathrm{T})$ and phase $(\varphi + \Psi)$ of the temperature distribution

across the surface of the LED from the four images collected during one modulation period. However, there are noises in the experiment. Therefore, in order to obtain high quality thermal images, averaging must be performed over many times (typically 20,000).

Thermoreflectance microscopy is a promising, high resolution, non-contact imaging technique. This technique provides high thermal resolution (10mK) and high spatial resolution (250nm) for thermal profiling and performance analysis of optoelectronic devices at the microscale [5]. It is critical for us to understand the temperature distribution and thermal characteristics of a device in order to improve its thermal management. Compared with infrared (IR) thermography, which is the most widely used thermal profiling technique, thermoreflectance microscopy technique has many advantages: it accept a broad range of wavelength, from 400nm to 1200nm; it has 250nm spatial resolution and 10mK thermal resolution; it only needs an ordinary glass lens which makes it inexpensive; it takes just minutes to provide the high thermal resolution lock-in thermography. However, the IR technique is expensive, and has low spatial resolution (1000nm) and low thermal resolution ($< 10\text{mK}$), and it is only effective on wavelength from 800nm to 1200nm [20]. Therefore, besides thermal mapping of LEDs, thermoreflectance microscopy technique has a great potential to be used in the industry for many applications, such as hot spot detection in electronic devices; quick analysis and thermal mapping of optoelectronic devices including vertical cavity surface emitting lasers (VCSELs) and solar cells;

providing information to traditional electrical device test. Figure 5.3.2 shows an example of the result from thermoreflectance microscopy. We are able to get the DC, phase, and ACDC image of the operating LED surface.

(a)

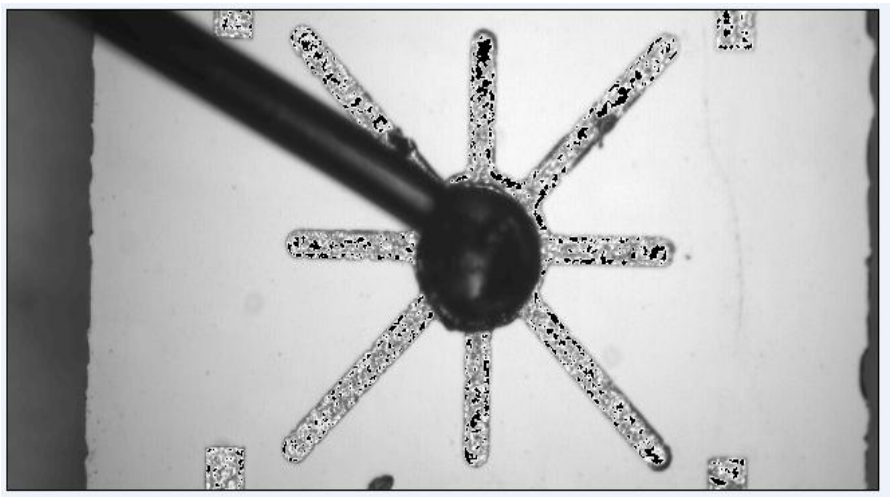

(b)

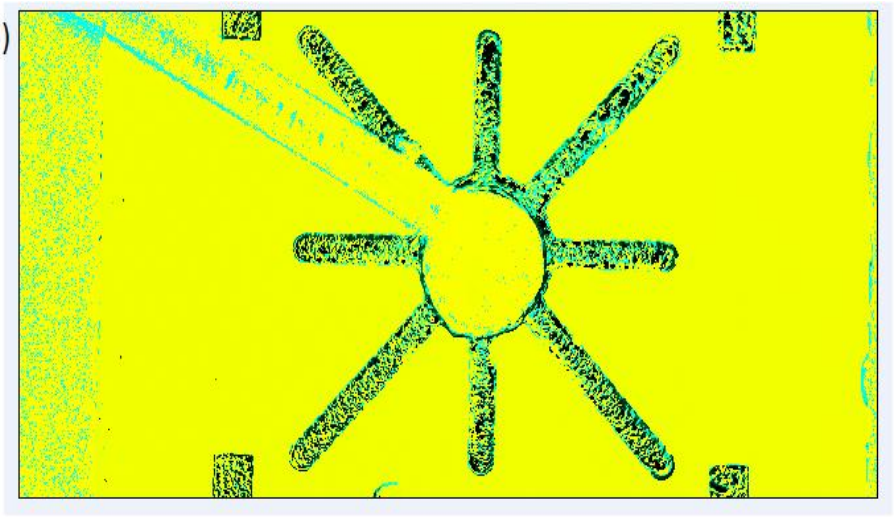

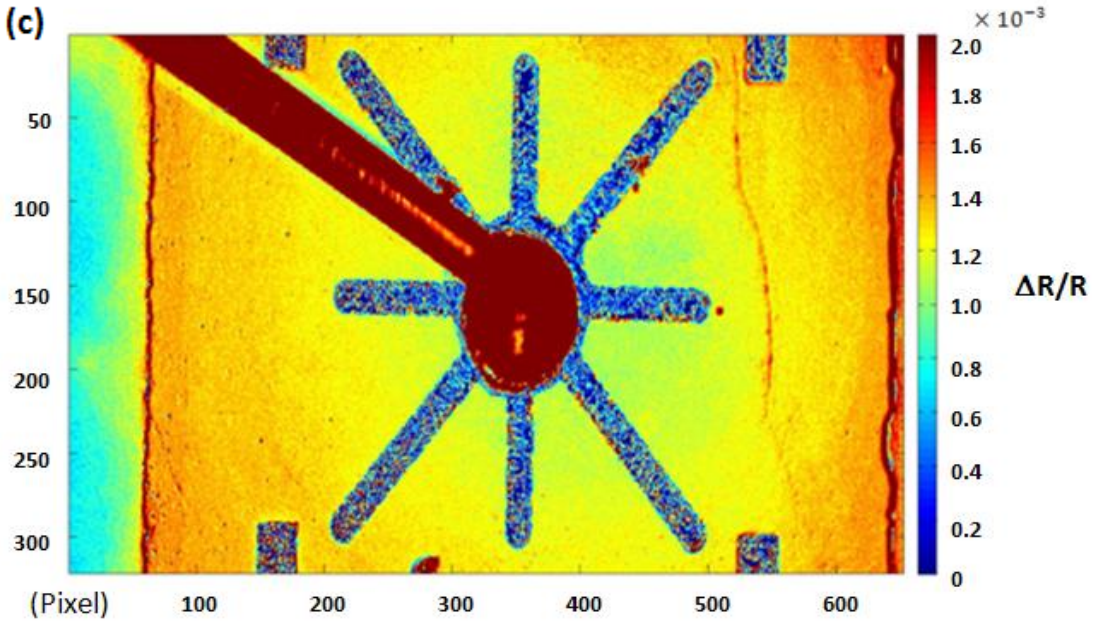

Figure5.3.2: (a) 2D DC (R) image of the de-encapsulated LED surface. (b) 2D Phase image of the de-encapsulated LED surface. (c) 2D AC/DC ($\Delta R/R$**) distribution across the operating de-encapsulated LED surface.**

4. Results and Discussions

This chapter describes the experimental results obtained for encapsulated and de-encapsulated Luxeon K2 Star Red LEDs. We first study the general characteristics of the LED: current-voltage (IV) curve, and the optical power-current (LI) curve.

As mentioned in the previous chapter, the main goals are: 1) measuring the thermal distribution inside the operating LED, both laterally and vertically in order to better understand the thermal performance of the LED; 2) apply a new technique of 2-Dimensional thermal mapping via thermoreflectance microscopy to obtain the first high resolution lateral temperature maps of the operating LED; 3) compare the results of the new thermoreflectance microscopy measurements with traditional methods of estimating the LED's temperature; 4) compare thermal performance of encapsulated and de-encapsulated LEDs. Therefore, in section 4.2, we study the spectrum of the encapsulated and de-encapsulated LED and measure the peak wavelength shift in order to obtain the p-n junction temperature. In section 4.3, we use the forward bias voltage measurement to obtain the average junction temperature for both devices. Furthermore, in section 4.4, we use thermoreflectance microscopy to generate the 2-Dimensional temperature distribution across the operating de-encapsulated LED surface.

Finally, we compare the three different temperatures of the de-encapsulated LED in order to understand the thermal performance of the LED.

4.1 Basic Characteristics: IV curve and LI curve

The current-voltage (IV) curves of the encapsulated LED and the de-encapsulated LED are obtained and are shown in Figure 4.1.1 (a), (b). The setup described in Chapter 3, Section 3.2 is used. For both devices, the case temperature is varied from 15℃ to 55℃ with a 5℃ increment by using the temperature controller. The applied current is changed from 0mA to 500mA with a 10mA increment by using the current source controlled by the LabVIEW program. Once the LED is turned on, the current increases sharply with the increasing forward voltage, as we expected. Moreover, in both Figure 4.1.1 (a) and (b), the forward voltage decreases with increasing case temperature at a fixed injection current.

The turn-on voltage for the encapsulated LED decreases from 1.9V to 1.75V as the case temperature increases. The turn-on voltage for the de-encapsulated LED decreases from 1.8V to 1.6V as the case temperature increases. Contrasting the turn-on voltage of the encapsulated and de-encapsulated LED, the data suggest that the de-encapsulated LED may be operating at a higher temperature

than is the encapsulated LED. This is an unusual result which will resurface in later measurement.

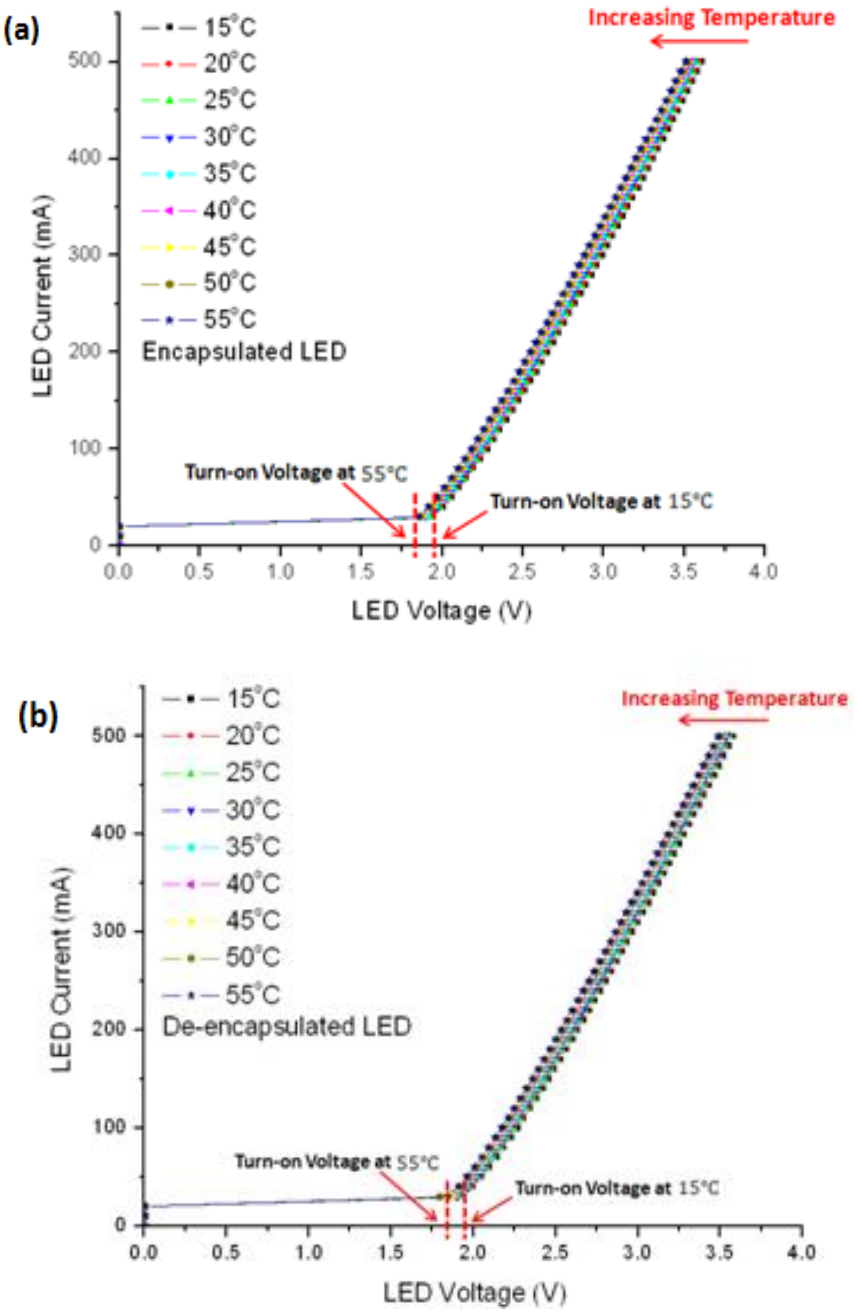

Figure 4.1.1 (a): Current-voltage (IV) curve for the encapsulated LED. (b): Current-voltage (IV) curve for de-encapsulated LED with case temperature changing from 15℃ to 55℃.

The emitted optical power versus applied electrical bias power curves are shown in Figure 4.1.2. This data is obtained by using the experimental setup and calibration technique in Chapter 3, Section 3.2.

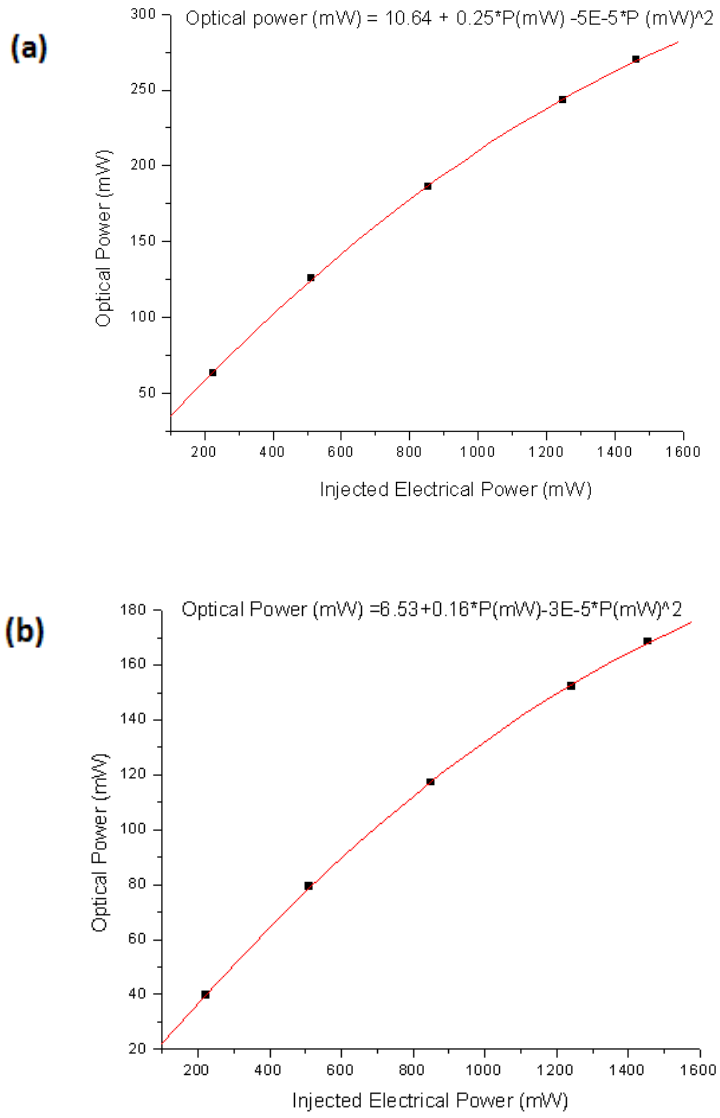

Figure 4.1.2 (a): Optical power vs. injected electrical power calibration for encapsulated LED with case temperature at 25℃. (b): Optical power vs. injected electrical power calibration for de-encapsulated LED with case temperature at 25℃.

The data are plotted in more traditional form as optical power versus electrical bias current (LI) in Figure 4.1.3 (a), (b). From both graphs, the optical power increases with drive current at a fixed case temperature, as we expected. We note, however, that at a fixed drive current, the optical power decreases with increasing case temperature. The decrease in optical power with increasing case temperature has been extensively noted in the literature [18], and is of great practical concern in the commercial development of LEDs.

Comparing the two graphs, the output optical power for the de-encapsulated LED is lower than the encapsulated LED under identical operating condition. This result suggests that the encapsulated silicone lens has a higher refractive index than the air and enhances the external quantum efficiency, therefore improves the light extraction. In addition, the optical power emission may be suppressed in the de-encapsulated LED which is operating at a higher temperature than is the encapsulated LED as suggested by the IV curves.

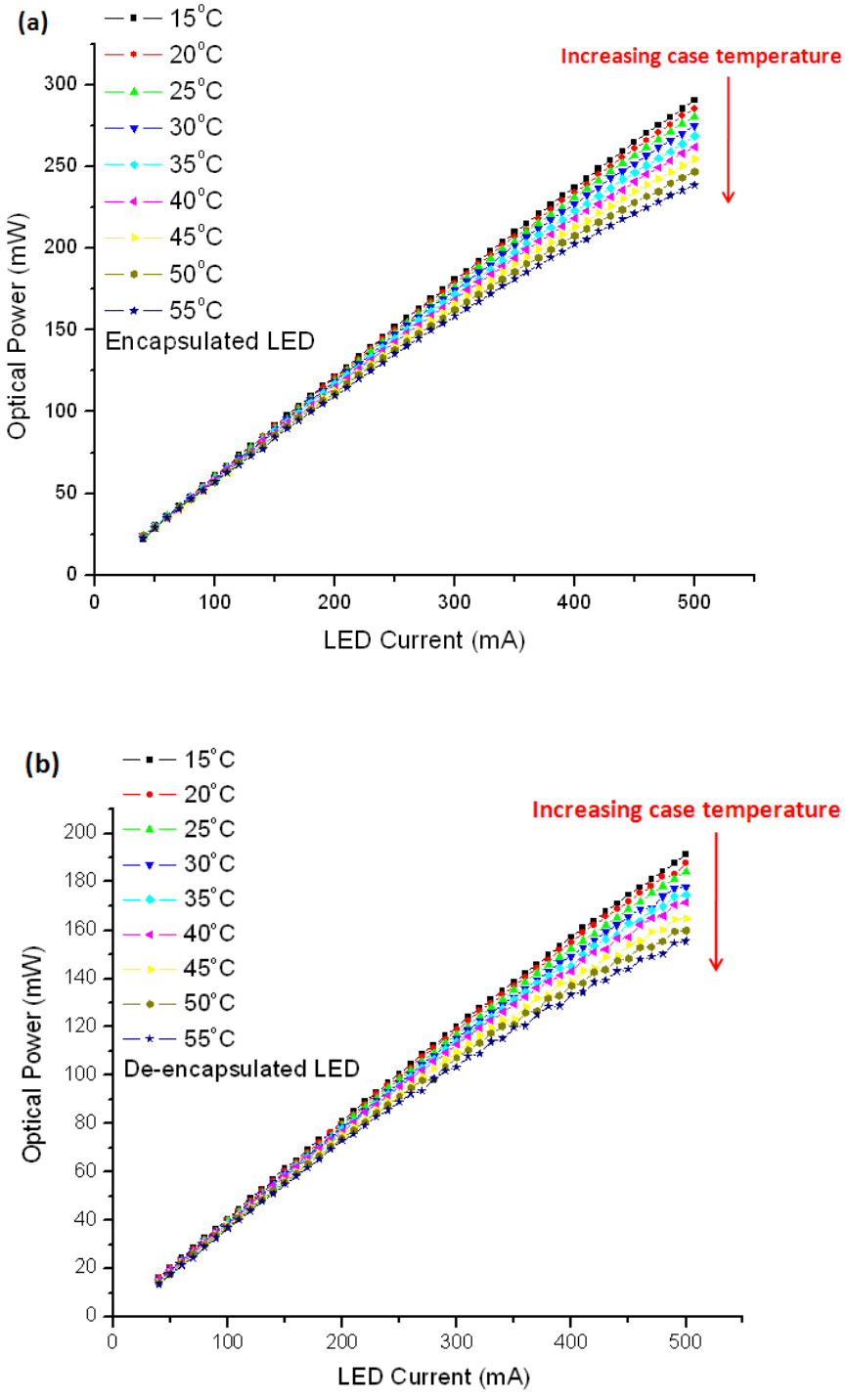

Figure 4.1.3 (a): Optical power-current (LI) curve of encapsulated LED with case temperature changing from 15℃ to 55℃. (b): Optical power-current (LI) curve of de-encapsulated LED with case temperature changing from 15℃ to 55℃.

4.2 Spectrum and Wavelength Length Shift Measurement

The spectra of the encapsulated LED and the de-encapsulated LED are obtained at various drive currents at case temperature of $25^{o}C$ as shown in Figure 4.2.1. The drive current is varied from 50mA to 450mA with a 100mA increment. For both devices, the spectra are red-shifted, and the intensity of the output light increases with increasing current, as we expected. As mentioned in Chapter 2, Section 2.4.4, high current increases the die temperature and hence decreases the bandgap energy which introduces a red shift to the spectrum. This red-shift of the operating wavelength with increasing case temperature has been previously noted in the literature [18], and has commercial concern because the output light color of the LED changes with temperature.

Figure 4.2.1 shows that the spectrum of the de-encapsulated LED is slightly red-shifted in comparison to the spectrum of the encapsulated LED at the same current. This shift suggests that the junction temperature of the de-encapsulated LED is slightly higher than the encapsulated LED, because at a fixed current, the greater the wavelength, the higher the junction temperature. This result is consistent with the IV and LI results shown earlier.

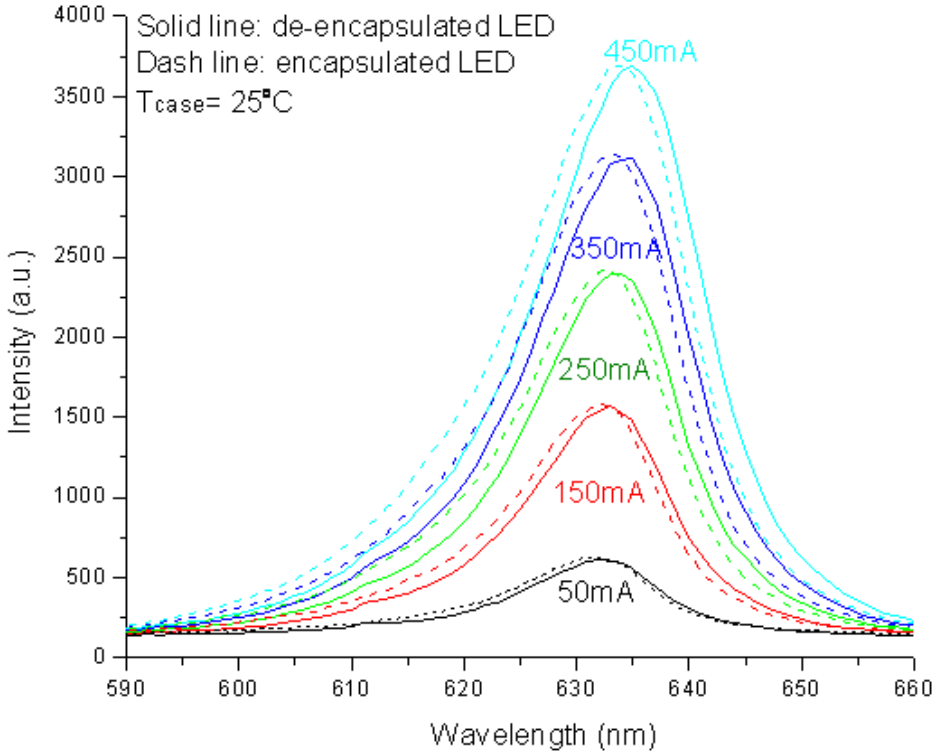

Figure 4.2.1: Spectra of encapsulated LED (solid lines) and de-encapsulated LED (dash lines) at different drive currents.

Peak wavelengths are obtained at various drive currents at case temperatures of 25℃, 35℃, and 45℃ for encapsulated LED and the de-encapsulated LED as shown in Figure 4.2.2. The drive current is from 50mA to 450mA with a 50mA increment. By recording the voltage across the LED, the injected electrical power is then calculated. As mentioned in Chapter 2, Section 2.4.4, the increasing current increases the temperature, therefore the peak wavelength increases for both devices. For the encapsulated LED, the peak wavelength increases from

637.5nm to 639.79nm, 639.39nm to 642.14nm, and 641.08nm to 643.74nm as the current increases from 50mA to 450mA at temperatures of $25^{o}C$, $35^{o}C$ and $45^{o}C$ respectively. We found that the peak wavelength and the injected electrical power have a linear relationship. As the injected electrical power increases, the peak wavelength is red-shifted at a fixed temperature.

Similarly, in the de-encapsulated LED case, the peak wavelength increases from 637.98nm to 640.68nm, from 639.57nm to 642.7nm, and from 641.31nm to 644.34nm at $25^{o}C$, $35^{o}C$, and $45^{o}C$ respectively as the current increases from 50mA to 450mA.

Figure 4.2.2 shows the comparison between the peak wavelength of the encapsulated LED and the de-encapsulated LED. The peak wavelength of the de-encapsulated LED is slightly greater than that of the encapsulated LED. This greater peak wavelength suggests that the de-encapsulated LED has a higher junction temperature than the encapsulated LED. Furthermore, compared the solid curve with the dash curve, the slope of de-encapsulated LED is greater than that of the encapsulated LED. This result suggests that the de-encapsulated LED can be heated up faster than the encapsulated LED due to the greater change in the wavelength.

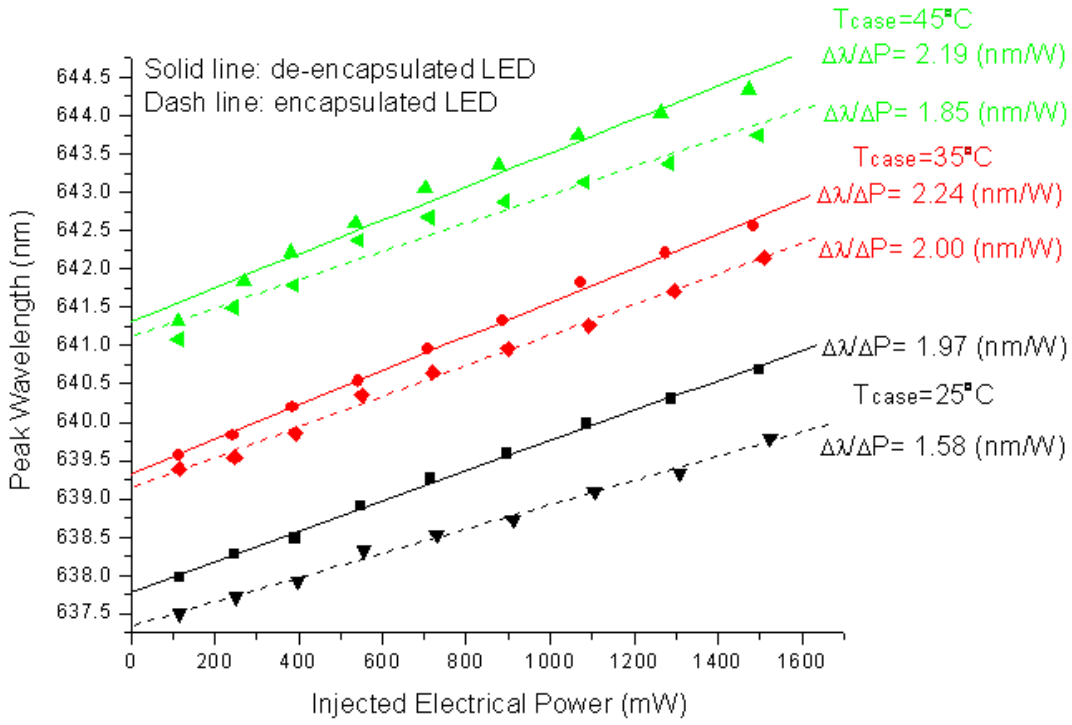

Figure 4.2.2: Peak wavelength vs. injected electrical power for encapsulated LED (dash lines) and de-encapsulated LED (solid lines).

The spectra for the encapsulated and de-encapsulated LED are obtained at various case temperatures with the same drive current of 20mA and are shown in Figure 4.2.3. The case temperature is varied from $15^{o}C$ to $55^{o}C$ with a $10^{o}C$ increment. For both devices, as mentioned in Chapter 2, Section 2.4.4, spectrum shifts to the higher wavelength with increasing case temperature. This result is expected because the increasing case temperature increases the die temperature, which decreases the bandgap energy, therefore resulting in a red-shift of the emitted light. The intensity of output light decreases as the case temperature

increases, due to the decrease in the forward voltage as explained in Chapter 2, Section 2.4.5. Figure 4.2.3 also shows that the spectrum of the de-encapsulated LED slightly shifts to the right in comparison to the spectrum of the encapsulated LED. This shift, although not obvious in this case due to the use of small applied current, is consistent with the peak wavelength measurement result that will be shown later.

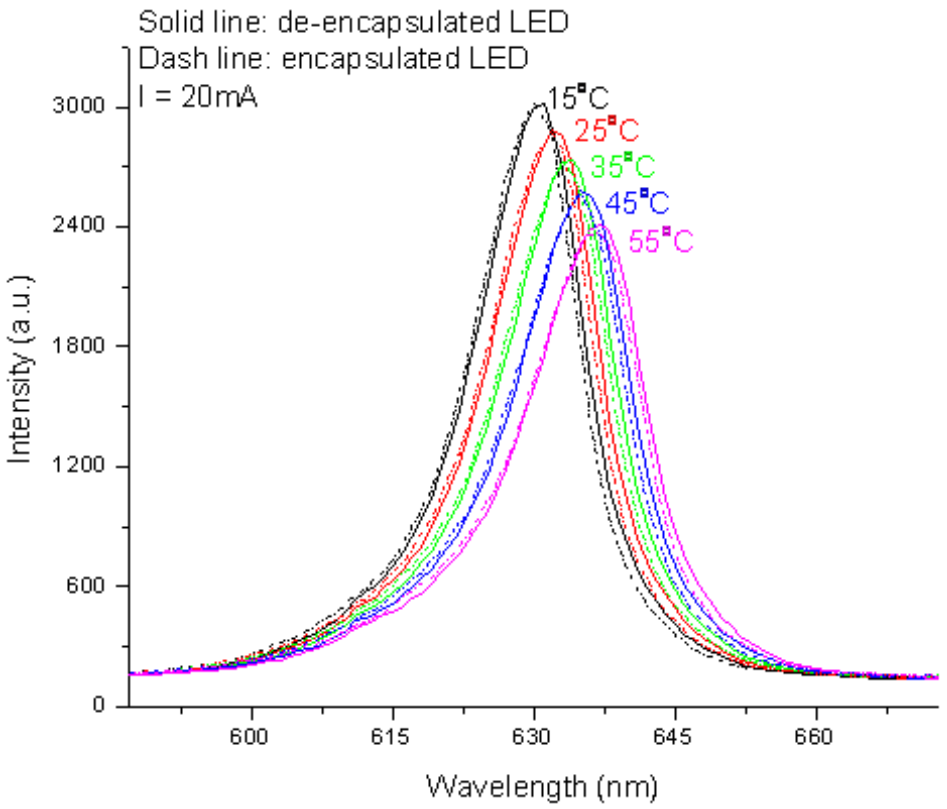

Figure 4.2.3: Spectrum of encapsulated LED (dash lines) and the de-encapsulated LED (solid lines) with different case temperature.

Figure 4.2.4 shows the comparison between the peak wavelength's of the encapsulated LED and the de-encapsulated LED at 5mA, 20mA, 100mA and 200mA drive current. The peak wavelength has a linearly proportional relationship with the case temperature. In addition, the peak wavelength of the de-encapsulated LED is always slightly higher than that of the encapsulated LED under identical conditions. This higher wavelength is further evidence that the de-encapsulated LED has a higher junction temperature than the encapsulated LED.

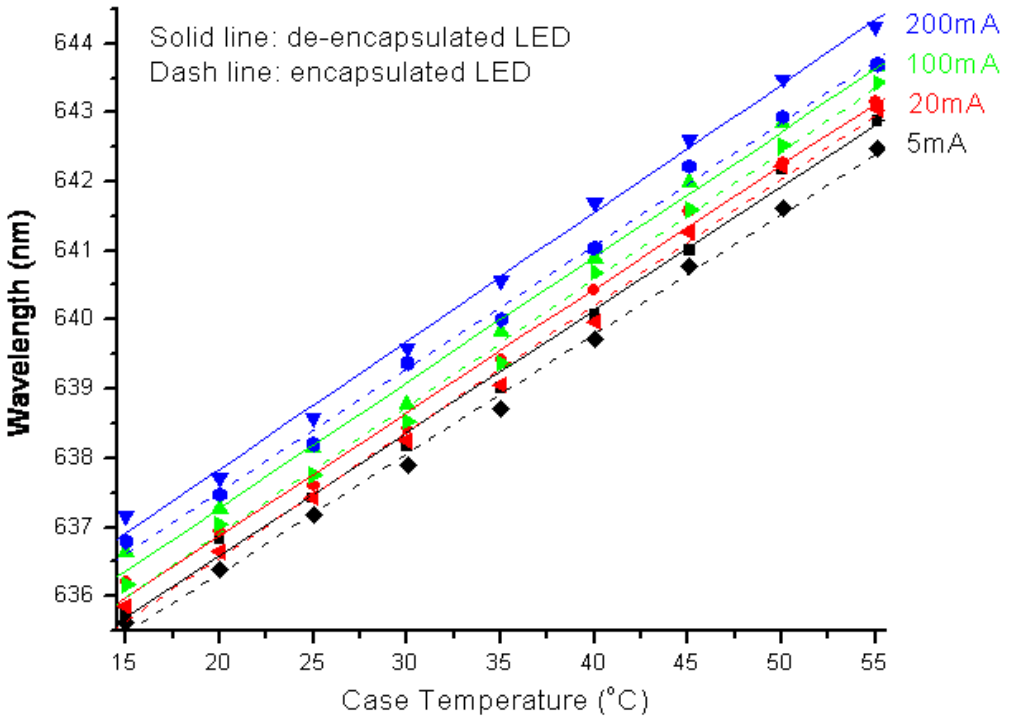

Figure 4.2.4: Wavelength versus case temperature for encapsulated LED and de-encapsulated LED with changing current from 5mA to 200mA.

As discussed, two relationships are obtained from the wavelength shift measurement: the wavelength versus injected electrical power (at fixed case temperature, Figure 4.2.2) and the wavelength versus case temperature (at fixed bias current, Figure 4.2.4). From those two equations, we can obtain the relationship between temperature and injected electrical power of the LED.

From Figure 4.2.2, we find the empirical relationship between peak wavelength and injected electrical power at $25^{o}\mathrm{C}$ case temperature for de-encapsulated LED:

$$\frac{\Delta\lambda}{\Delta p} = 1.97\ (\frac{\mathrm{nm}}{\mathrm{W}}). \qquad (4.2.1)$$

This slope varies very slightly with case temperature. Throughout our measurements, we set the case temperature at 25℃.

From Figure 4.2.4, we notice that the slope of the wavelength versus temperature is independent of the choice of bias current:

$$\frac{\Delta\lambda}{\Delta T} = 0.2\ (\mathrm{nm}/℃). \qquad (4.2.2)$$

Therefore, we substitute Eq. 4.2.1 into Eq 4.2.2 and find the change in temperature due to injected electrical power at case temperature of 25℃:

$$\frac{\Delta T}{\Delta P} = 10\ (℃/\mathrm{W}). \qquad (4.2.3)$$

Likewise, at a case temperature of 25℃, the temperature of the encapsulated LED is found to vary with injected electrical power as:

$$\frac{\Delta T}{\Delta P} = 8\ (℃/W). \qquad (4.2.4)$$

Figure 4.2.5 shows the dependence of junction temperature on injected electrical power for the two types of LEDs.

Once again, the results show that the de-encapsulated LED has a slightly higher junction temperature than the encapsulated LED, which is consistent with our earlier independent results.

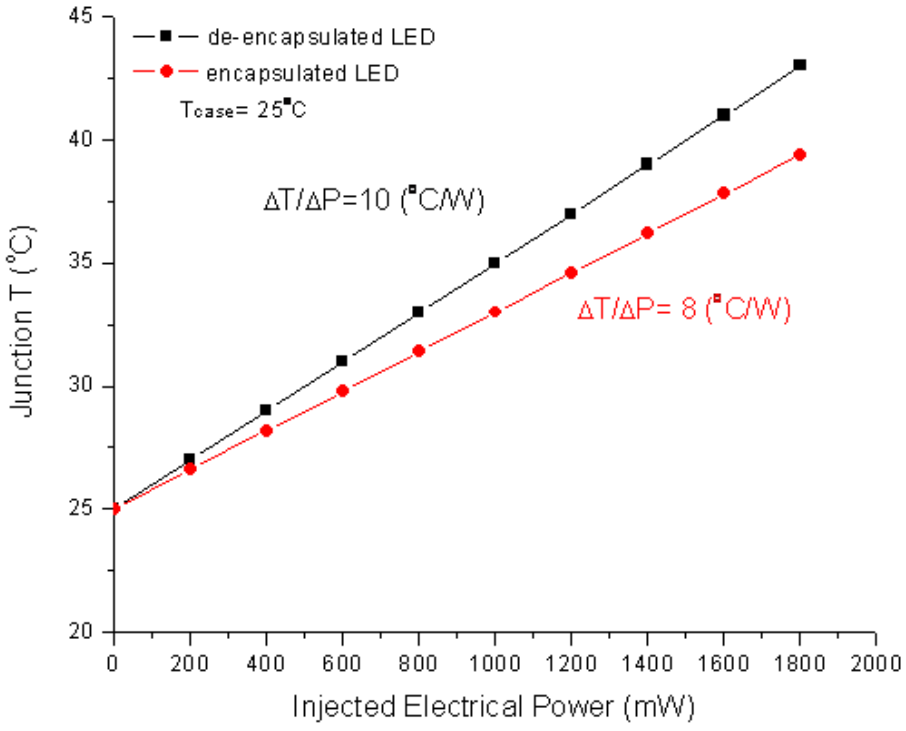

Figure 4.2.5: Junction temperature vs. injected electrical power for encapsulated LED and de-encapsulated LED; data extracted from wavelength shift measurement.

4.3 Forward Voltage Measurement

In order to calibrate this technique, as described in Chapter 3, Section 3.4, the relationship between the forward voltage and the case temperature for the encapsulated LED and the de-encapsulated LED is plotted in Figure 4.3.1. The drive currents are 1mA, 2.5mA and 5mA, which are low enough to minimize the self-heating in the p-n junction as discussed in Chapter 3.

As the temperature increases, the forward voltage decreases as discussed in Chapter 2, Section 2.4.5. The calibration coefficient α, which is defined as the applied voltage divided by the case temperature, is obtained by doing the linear fit of the taken points. α is $-2.24\,\mathrm{mV/°C}$, $-2.16\,\mathrm{mV/°C}$, and $-2.15\,\mathrm{mV/°C}$ for encapsulated LED, and $-2.31\,\mathrm{mV/°C}$, $-2.22\,\mathrm{mV/°C}$, and $-2.22\,\mathrm{mV/°C}$ for de-encapsulated LED with drive current at 1mA, 2.5mA and 5mA respectively.

Figure 4.3.1 shows that at the same temperature, the forward voltage of the encapsulated LED is slightly higher than that of the de-encapsulated LED at the same drive current. This suggests once again that the temperature of the de-encapsulated LED is higher than the temperature of the encapsulated LED.

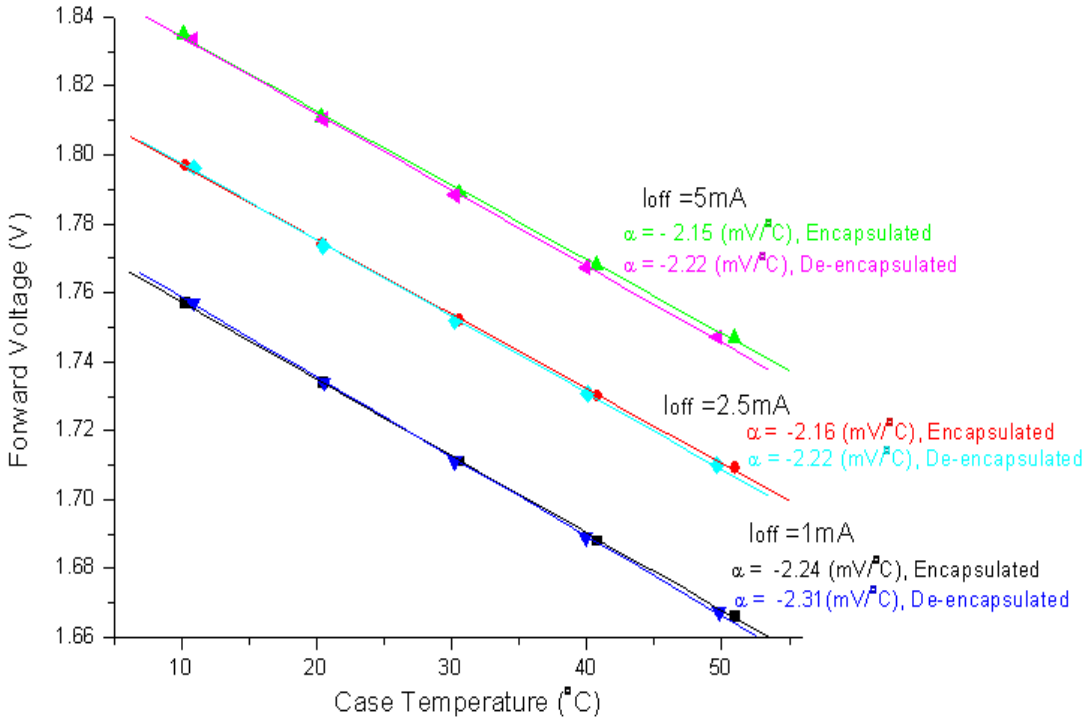

Figure 4.3.1: Forward voltage vs. junction temperature calibration of encapsulated LED and de-encapsulated LED.

Figure 4.3.2 (a) shows the raw measured voltage versus time data obtained from the pulsed current measurement, as discussed in Chapter 3, Section 3.4. The frequency is 1Hz and the duty cycle is 0.02% which provides a 200μs pulsed period. The black color curve is a DC signal with 5mA current. It is recorded as a reference voltage for calculating the change in forward voltage later. The high operating currents are at 469.94mA, 357.15mA, 254.14mA, 150.55mA, and 56.39mA, with low current at 5mA, which corresponds to the calibration current used in Figure 4.3.1.

Figure 4.3.2 (b) is the analyzed data obtained by smoothing-advanced averaging (number of points=500) the row data shown in Figure 4.3.2 (a). The reference voltage at 5mA and the forward bias voltage when the high operating current is pulsed down to 5mA, are measured from the curves at the off-state of the applied pulses, as shown in the zoom-in view of Figure 4.3.2 (c). Reference voltage is 2.076V. For the pulses cases, the off-state voltage are 2.073V, 2.069V, 2.057V, 2.048V, and 2.034V with the corresponding high operating current at 56.39mA, 150.55mA, 254.14mA, 357.15mA, and 469.94mA, as shown in Figure 4.3.2 (d). As we can see, the off-state voltage decreases as the maximum applied current increases.

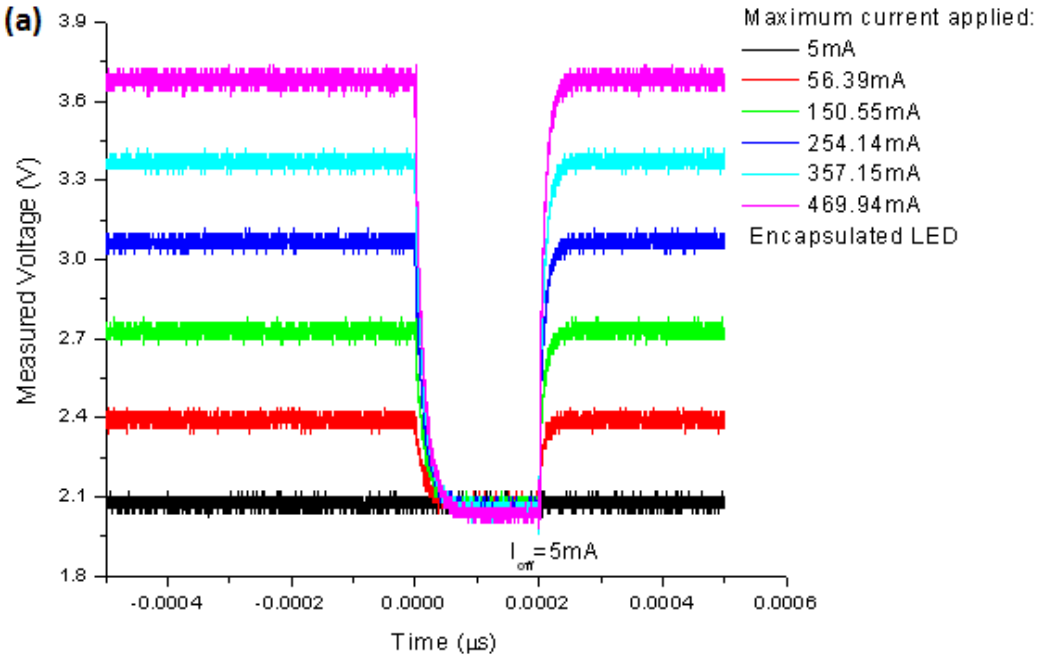

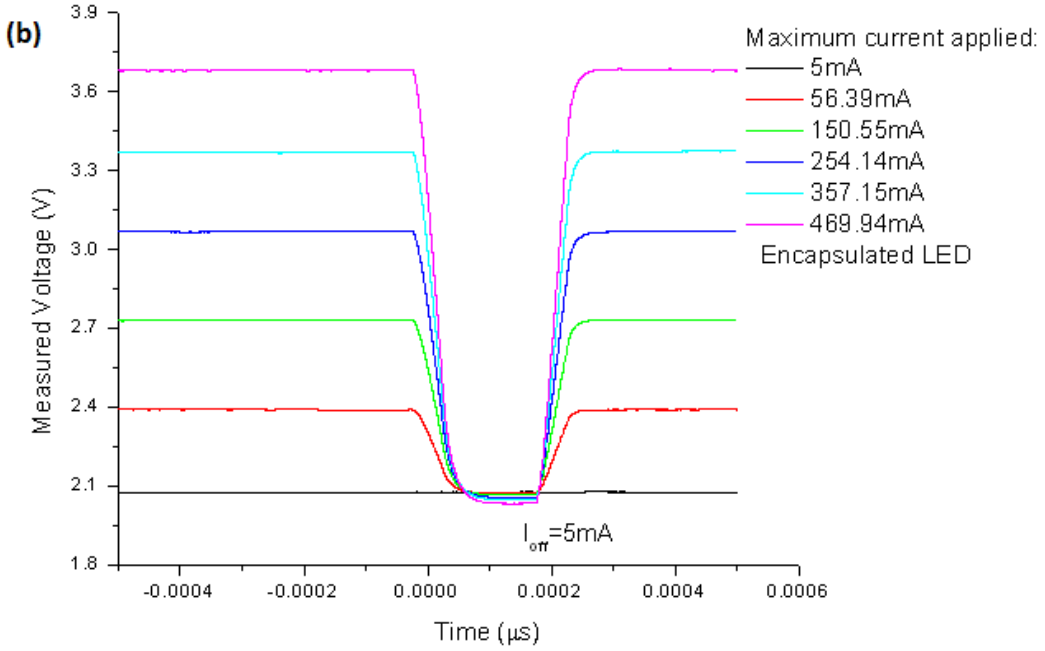
(b)
Maximum current applied:
5mA
56.39mA
150.55mA
254.14mA
357.15mA
469.94mA
Encapsulated LED
Measured Voltage (V)
3.9
3.6
3.3
3.0
2.7
2.4
2.1
1.8
-0.0004
-0.0002
0.0000
0.0002
0.0004
0.0006
Time (μs)
I_off=5mA

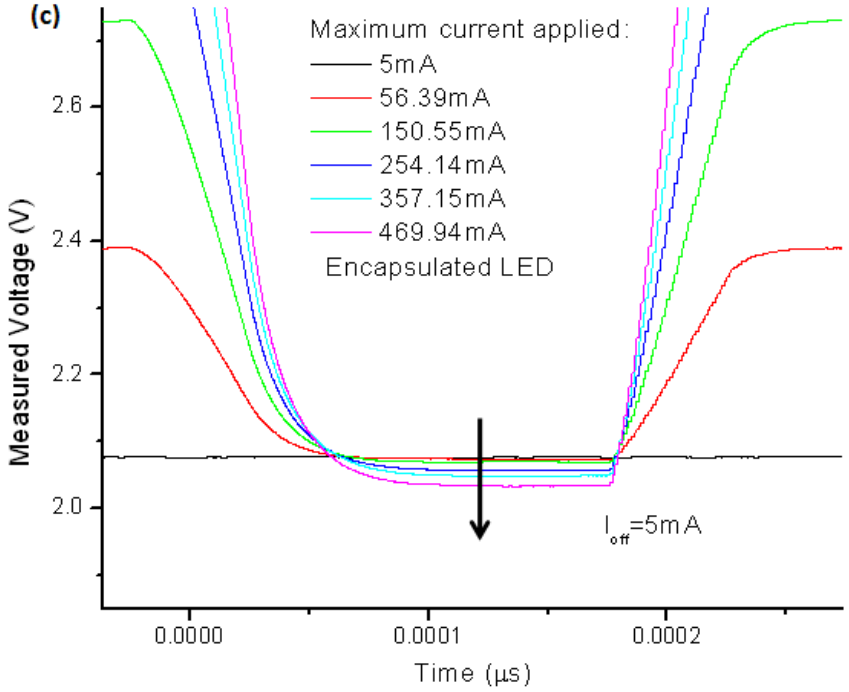
(c)
Maximum current applied:
5mA
56.39mA
150.55mA
254.14mA
357.15mA
469.94mA
Encapsulated LED
Measured Voltage (V)
2.6
2.4
2.2
2.0
0.0000
0.0001
0.0002
Time (μs)
I_off=5mA

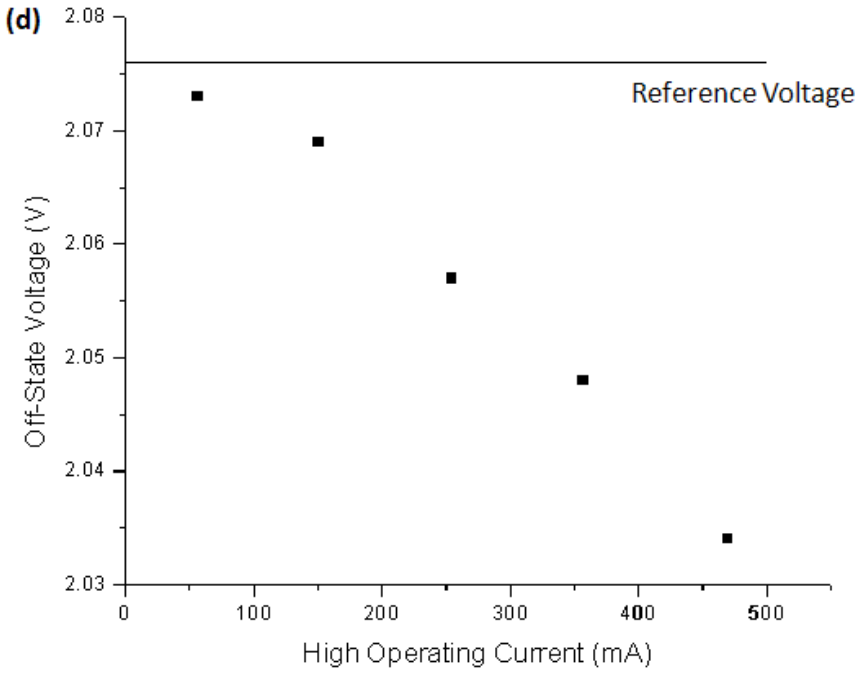

Figure 4.3.2 (a): Forward voltage drop measurement (Raw data) of encapsulated LED with 5mA off-state current. (b): Forward voltage drop measurement (smoothed data). (c): Forward voltage drop measurement (smoothed data, zoom in). (d): Measured off-state voltage versus high operating current and the measured reference voltage.

In the reference voltage measurement, the LED is operated at a very low current, so the operating temperature should be roughly the case temperature. When the LED is operated at high current, the operating temperature is the case temperature plus some additional contribution. The change in the temperature (ΔT) is proportional to the bias electrical power. Hence, when the LED is briefly pulsed off, with no time for ΔT to be dissipated, the measured junction voltage will be

the reference voltage minus the change in the forward voltage ($V_{ref} - \Delta V_f$), where ΔV_f is the offset due to the change in the temperature (ΔT).

The change in the forward voltage (ΔV_f) can be calculated by using the off-state voltage minus the reference voltage. The change in the temperature (ΔT) can be calculated by:

$$\Delta T = \Delta V_f / \alpha \ . \qquad (4.3.1)$$

where α = - 2.15 (mV/℃) is the calibration coefficient calculated from Figure 4.3.1. Injected electrical power is calculated by using the high operating current multiplied by the corresponding voltage. Figure 4.3.3 shows the empirical relation between the change in temperature and the injected electrical power.

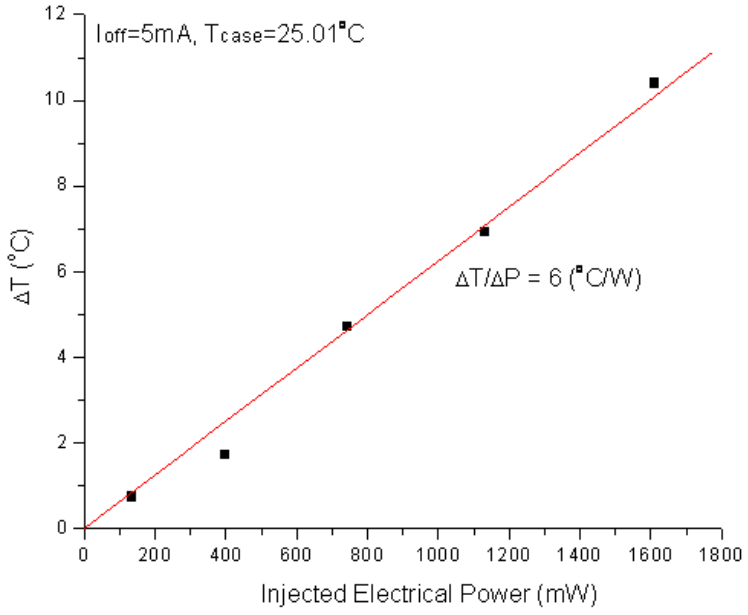

Figure 4.3.3: ΔT vs. injected electrical power of encapsulated LED with 5mA off-state current.

Based on the discussion above, the average operating temperature can be obtained by adding ΔT and the case temperature:

$$T = T_{case} + \Delta T \ . \qquad (4.3.2)$$

Similarly, the temperatures are obtained for the encapsulated LED with 1mA pulsed current and the de-encapsulated LED with 5mA and 1mA pulsed current. Figure 4.3.4 (a) and (b) show the comparison between encapsulated LED and de-encapsulated LED with 5mA and 1mA off-state current. Both graphs show that the encapsulated LED operates at a lower average temperature than the de-encapsulated LED.

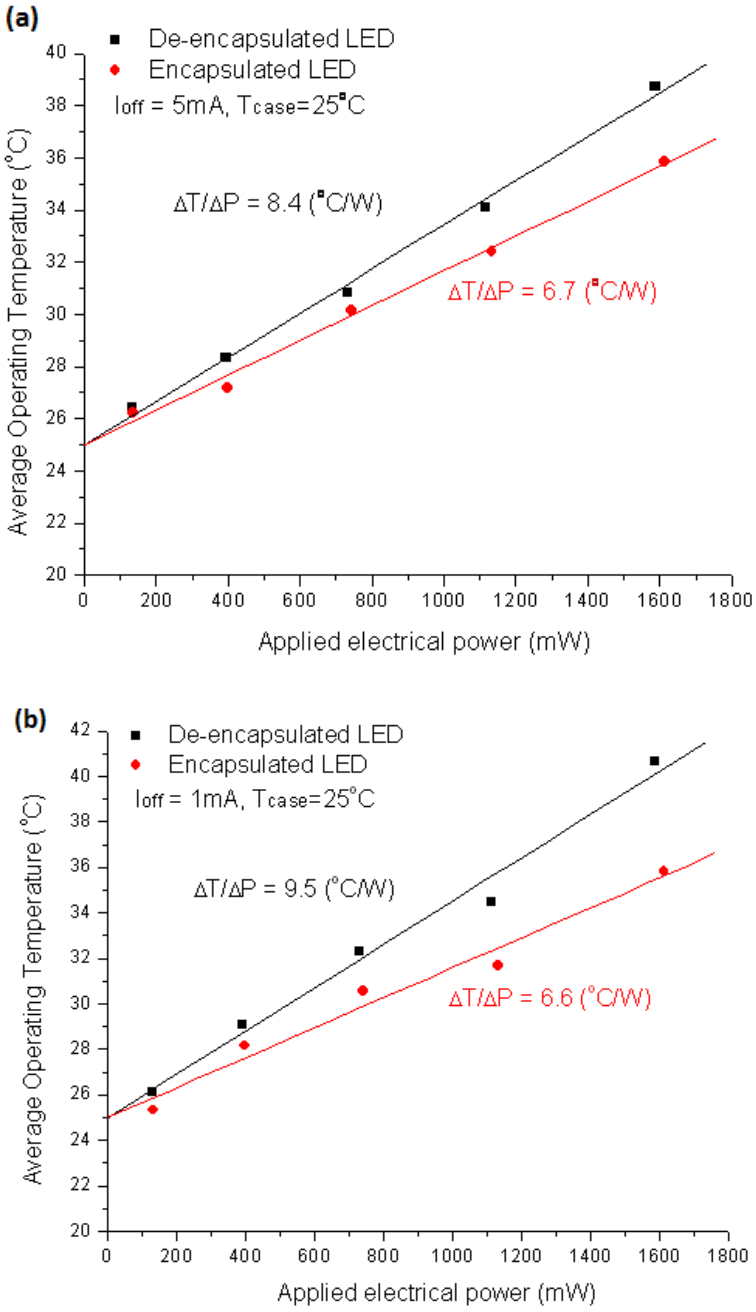

Figure 4.3.4 (a): Temperature vs. applied electrical power of the encapsulated LED and the de-encapsulated LED with 5mA off-state current. (b): Temperature vs. applied electrical power of the encapsulated LED and the de-encapsulated LED with 1mA off-state current.

4.4 Thermoreflectance Microscopy

By using the thermoreflectance microscopy setup in Chapter 3, Section 3.5, surface temperature of the operating de-encapsulated LED is obtained. Figure 4.4.1 is a 2D map of $\frac{\Delta R}{R}$ across the operating de-encapsulated LED surface. The LED is operated with a sinusoidal current which has a maximum current at 474.68mA and a minimum current at 0.44mA and the modulation frequency is at 10Hz. According to the four bucket integration technique discussed in Chapter 2, the CCD camera is triggered at frequency at 40Hz. Different colors represent the relative change in the reflectivity ($\frac{\Delta R}{R}$).

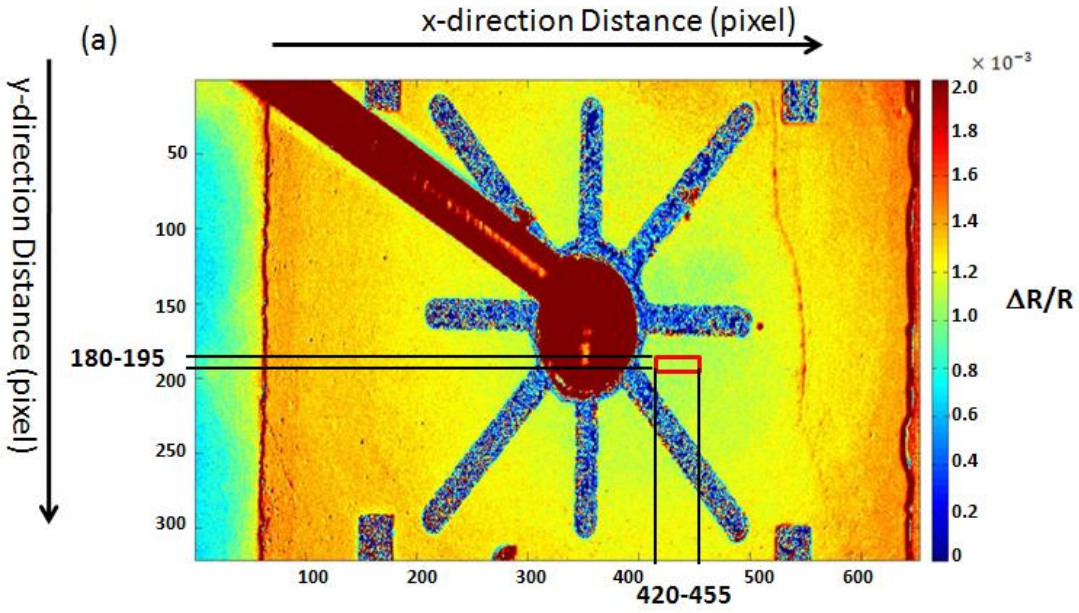

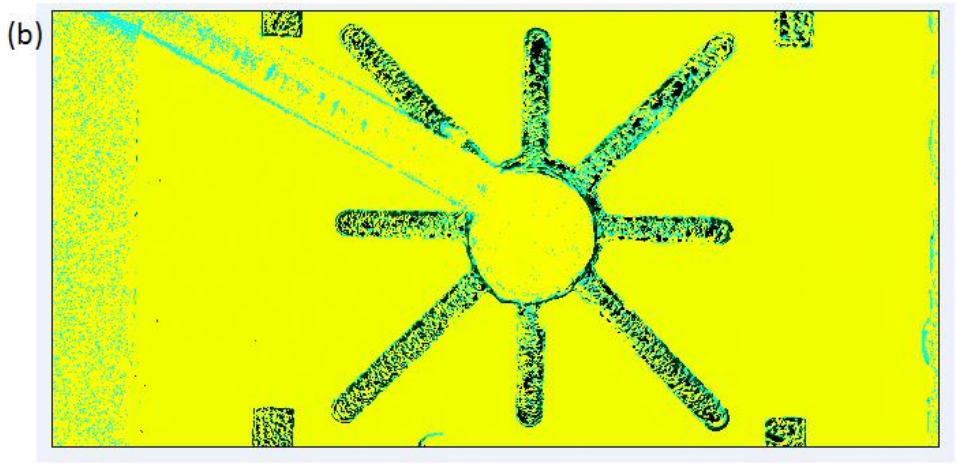

Figure 4.4.1: (a) 2D $\Delta R/R$ distribution across the operating de-encapsulated LED surface with 474.68mA maximum current. (b) Phase image of the operating de-encapsulated LED.

4.4.1 Spatial Variation of ΔT

Figure 4.4.2 shows the temperature distribution along the vertical direction of the LED chip. The green curve is the temperature at position x=630 (pixel), the red curve is the temperature at position x= 450 (pixel), and the black curve is the temperature at position x= 415 (pixel). Each curve shows a higher temperature at the top and bottom of the graph on the vertical distance than that at the center. Comparing the three curves, the temperature at 630 pixels is higher than that of 450 pixels and 415 pixels. These results suggest that the temperature of the LED edge is higher than that of the LED center. We attribute this temperature distribution to two heat generation mechanisms: 1) According to Figure 4.4.3, there is non-radiative recombination at the leaning face of the inverted pyramid

structure of the LED. The non-radiative recombination produces heat which increases the temperature at the edge of the LED surface. 2) The grater shunt resistance at the edge of the pyramid produces the more resistive heating to the top surface edge.

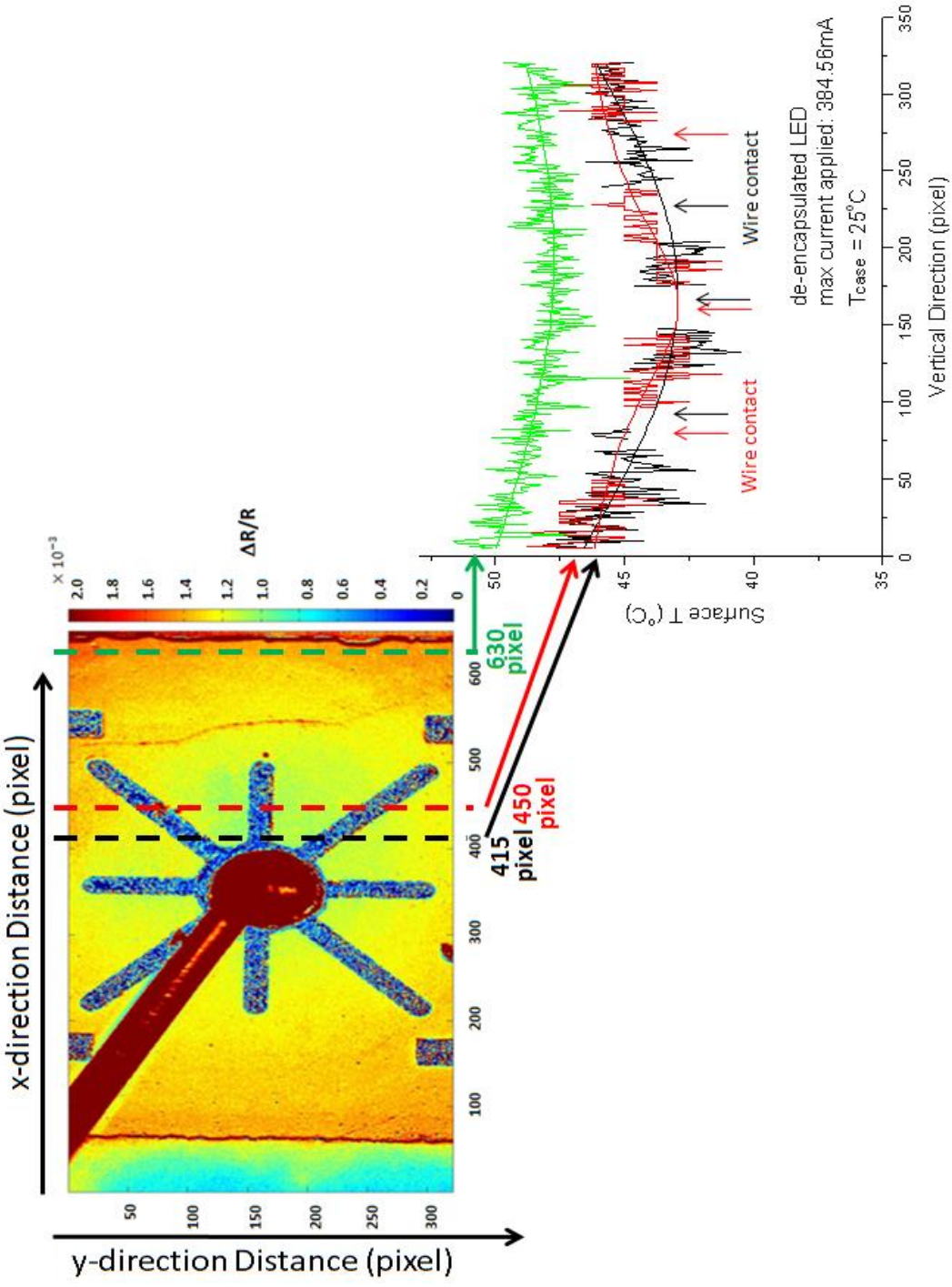

Figure 4.4.2: Spatial variation of ΔT at 415 pixel, 450 pixel and 630 pixel.

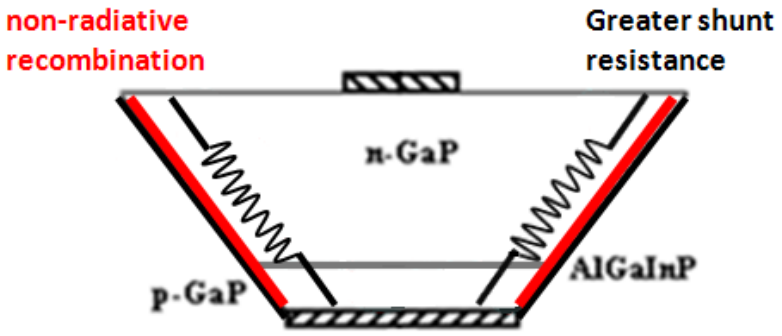

Figure 4.4.3: Heat generation mechanisms attribute to the higher edge temperature than that of the center.

4.4.2 Surface Temperature vs. Applied Electrical Power

Five thermal mappings are obtained under five different sinusoidal currents. The amplitude of the drive currents are 51.93mA, 146.99mA, 289.41mA, 384.56mA and 474.68mA respectively. As shown in Figure 4.4.1, by choosing the same area (pixel: 180-195 and 420-455) on each of the thermal mapping, $\overline{\Delta R \,/\, R}$ for this region under different drive currents is calculated. Based on:

$$\frac{\Delta R}{R} = \left(\frac{1}{R}\frac{\partial R}{\partial T}\right)\Delta T = \kappa \Delta T \qquad (4.4.1)$$

the amplitude of the surface temperature modulation can then be calculated. The temperature calibration coefficient κ equals $8e^{-5}(K^{-1})$ for Gallium Phosphide material which is the n-type material for the Luxeon K2 Start Red LED that we used in this project [9].

We expect that the amplitude of the temperature modulation ΔT should scale linearly with the amplitude of the electrical power modulation ΔP. Because the IV curve of an LED is nonlinear, some careful thought is required to correctly calculate ΔP.

For the sinusoidal applied current, the current and the voltage can be expressed in the equations below:

$$I = I_0 + \Delta I e^{i\omega t} \tag{4.4.2}$$

$$V = V_0 + \Delta V e^{i\omega t}. \tag{4.4.3}$$

Hence the injected electrical power is given by:

$$\begin{aligned} P = IV &= \left(I_0 + \Delta I e^{i\omega t}\right)\left(V_0 + \Delta V e^{i\omega t}\right) \\ &= I_0 V_0 + [(\Delta I)V_0 + I_0(\Delta V)]e^{i\omega t} + \Delta I \Delta V e^{i2\omega t}. \end{aligned} \tag{4.4.4}$$

The CCD camera is at 4f = 4($\frac{\omega}{2\pi}$), so the four bucket integration technique (discussed in Chapter 3, Section 3.5) locks onto the signal at f = $\frac{\omega}{2\pi}$. Hence only the part that corresponds to the $e^{i\omega t}$ contributes to the measured signal:

$$\Delta P = (\Delta I)V_0 + I_0\,(\Delta V)$$

$$= (I_{max} - I_{min})\left(\frac{V_{max} + V_{min}}{2}\right) + \left(\frac{I_{max} + I_{min}}{2}\right)(V_{max} - V_{min}) \qquad (4.4.5)$$

Therefore, ΔP can be calculated by recording the maximum and minimum current and voltage of the sine wave. Figure 4.4.4 shows the plot of ΔT versus the change in the injected electrical power.

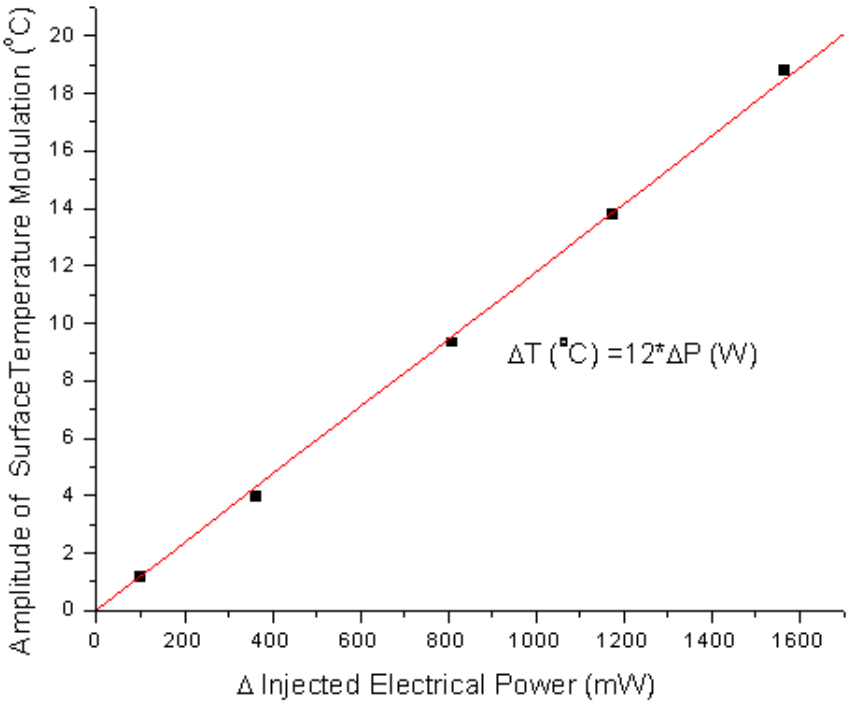

Figure 4.4.4: Change in surface temperature vs. change in injected electrical power of de-encapsulated LED at case temperature 25℃ with temperature calibration coefficient $\kappa = 8 \times 10^{-5}(K^{-1})$. (This result is measured from LED sample 1. Previous results are measured from LED sample 2.)

The case temperature is $25℃$ when the LED is turned off. Therefore, the actual surface temperature under operating conditions is:

$$T = \Delta T + 25℃ \ . \tag{4.4.6}$$

Since the minimum injected electrical powers for the five different sinusoidal currents are approximate zero, the corresponding injected electrical power to the temperature in Eq. 4.4.6 can be assumed as the maximum current times the maximum voltage. Figure 4.4.5 shows the plot of surface temperature versus injected electrical power.

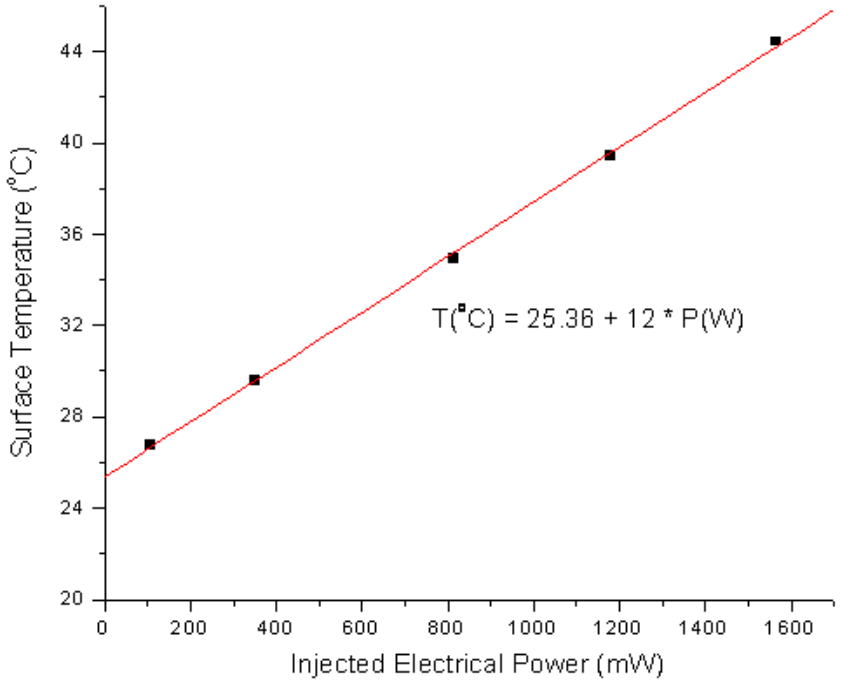

Figure 4.4.5: Surface temperature vs. injected electrical power of de-encapsulated LED with temperature calibration coefficient $\kappa = 8 \times 10^{-5}(K^{-1})$ at case temperature of $25℃$. (This result is measured from the LED sample 1. Previous results are measured from LED sample 2.)

4.5 Comparison of the Three Temperature Measurement Techniques

Figure 4.5.1 shows the comparison between our results for the three methods of temperature measurement: wavelength shift measurement, which measures the p-n junction temperature; forward bias voltage measurement, which measures the average temperature across the device; and thermoreflectance microscopy, which measures the surface temperature.

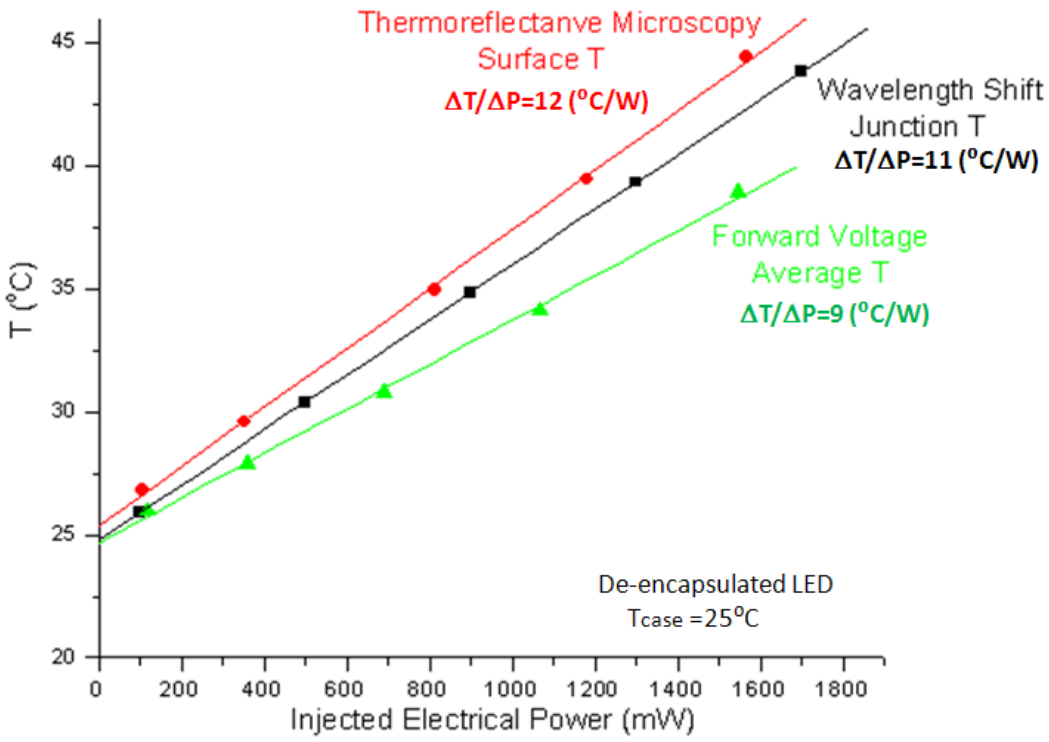

Figure 4.5.1: Comparison of the three temperature measurements. (These results are measured from the LED sample 1. Previous results are measured from LED sample 2.)

For these three measurements, the temperature has a linear relationship with the injected electrical power as we expected. The surface temperature is slightly higher than the junction temperature. We attribute this higher surface temperature to two heat generation mechanisms: 1) the non-radiative recombination at the top corner of the LED; 2) the contact resistance of the bond at the surface connection, as shown in Figure 4.5.2. The junction temperature is slightly higher than the average operating temperature. The possible reason for the higher junction temperature than the average operating temperature could be that the heatsink attached to the LED chip. The heatsink conducts the heat efficiently to the packaging which decreases the temperature at the bottom. The bottom temperature is much lower than the junction temperature, therefore the average operating temperature is lower than the junction temperature.

In addition, the surface temperature in this plot is an underestimate of the surface temperature, because we choose the coolest point on the surface, as shown in Figure 4.4.1.

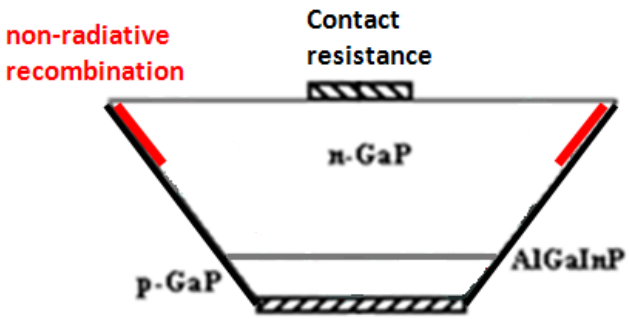

Figure 4.5.2: Heat generation mechanisms attribute to the higher surface temperature.

5. Conclusions

In summary, we have characterized and thermally profiled two types of LEDs: the encapsulated and de-encapsulated Luxeon K2 Star Red LED. Three independent techniques are used to measure the temperature of the operating devices. The conclusions drawn from this project are presented below.

We have fully electronically and optically characterized both the encapsulated and de-encapsulated LED via standard techniques. The current-voltage (IV) curves indicate that both types of devices have similar IV characteristics. Furthermore, for both types of devices, the forward voltage decreases with increasing case temperature at a fixed drive current. This degradation in electrical performance with case temperature has been previously noted in the literature [19]. The optical power-current (LI) curves show that for both types of devices, the optical power decreases with increasing case temperature at a fixed drive current. This thermal degradation of the optical performance has been previously noted in the literature [19]. In addition, the optical power emitted by the de-encapsulated LED is lower than that of the encapsulated LED at a fixed case temperature and a fixed drive current, as we expected. This result indicates that: 1) the silicone encapsulant has a higher refractive index than the air; therefore, the external quantum efficiency is

enhanced. Hence more photons are emitted [15]; 2) the silicone lens help to collimate the emitted light, therefore, more photons can be detected by the equipment. The spectra of both types of devices are red-shifted in response to the increase in case temperature and the increase in drive current, as we expected. This red-shift suggests that the light output degradation can be predicted by measuring the peak wavelength shift, and it has been previously noted in the literature [4].

Based on the results from the wavelength shift measurement and forward bias voltage measurement, we find that the temperature of the encapsulated LED is lower than that of the de-encapsulated LED under identical operating conditions. As we know for LED, the convection is an ineffective method of heat extraction, but conduction is a much effective method due to the small size of the LED chip and the use of heat sink. Therefore, a possible reason could be that the silicone encapsulant and lens help to conduct the heat from the active region of the LED device to the ambient. This result is somewhat surprising to us because the conventional thought is that LEDs are encapsulated in a transparent resin, which is a poor thermal conductor [16]. However, actually, the silicone encapsulant has a high thermal conductivity around 0.3 to 2.5 W/mK [17]. This

high thermal conductivity makes silicone lens and encapsulant a good heat spreader.

The wavelength shift measurement, forward bias voltage measurement and thermoreflectance microscopy, measure the temperature of the LED at subtly different locations. Wavelength shift measurement measures the junction temperature, forward bias voltage measurement measures the average operating temperature inside the LED device, and thermoreflectance microscopy measures the surface temperature of the operating LED. Based on our experimental results using these three techniques, we find that the surface temperature is slightly higher than the p-n junction temperature, which is slightly higher than the average LED temperature. This result indicates that thermoreflectance microscopy is quantitatively consistent with the two traditional temperature measurements. Moreover, we are able to obtain a 3-Dimensional temperature profile. Figure 5.1 is a vertical temperature profile, and the lateral temperature profile is obtained from thermoreflectance microscopy (Figure 4.4.1 (a)). They together provide us the 3D temperature profile. We attribute the higher surface temperature to two heat generation mechanisms: 1) the non-radiative recombination at the top corner of the LED; 2) the contact resistance of the bond at the surface connection, as shown in Figure 4.5.2. The possible reason for the higher junction temperature

than the average operating temperature could be that the heatsink attached to the LED chip. The heatsink conducts the heat efficiently to the packaging which decreases the temperature at the bottom. The bottom temperature is much lower than the junction temperature, therefore the average operating temperature is lower than the junction temperature.

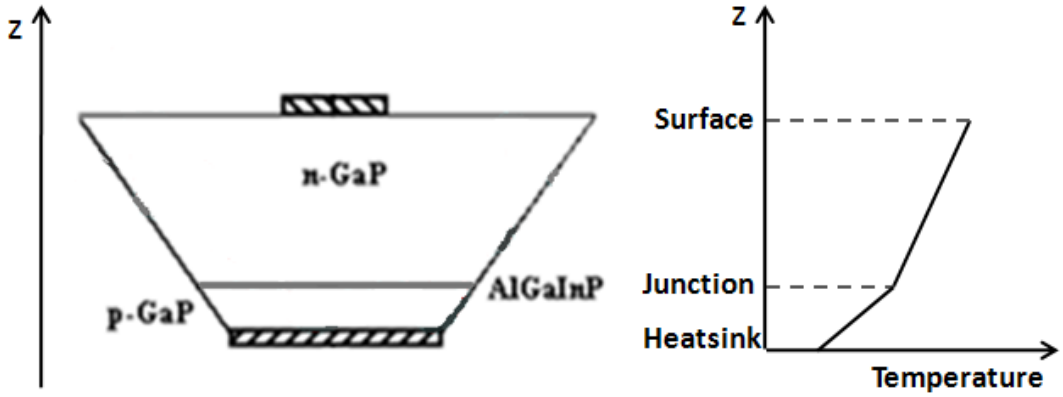

Figure 5.1: Schematic of vertical temperature profile of the LED.

Furthermore, thermoreflectance microscopy is used to measure the 2-Dimensional temperature distribution across the LED surface with 250nm spatial resolution and 10mK thermal resolution. This thermal mapping indicates that the temperature of the LED chip edge is higher than that of the center. This is a significant result that has not been previous reported in the literature. We have discussed two possible reasons: the non-radiative recombination and the greater shunt resistance at the leaning face of the inverted pyramid structure.

Overall, several temperature measurement techniques have been used to investigate the thermal management of the encapsulated and de-encapsulated LED. Our conclusions are: 1) the silicone encapsulant and lens improve thermal performance of the LED, presumably by acting as a heat spreader; 2) thermoreflectance microscopy is quantitatively consistent with traditional bulk and average temperature measurements, but offers the large advantage of enabling lateral 2-Dimensional thermal mapping with spatial resolution of 250nm. From this technique, we find for the first time that the edges of the LED surface are hotter than the center; 3) the use of three independent means of temperature characterization enables us to extract information about how temperature varies vertically. The fact that the surface temperature is higher than the junction temperature is consistent with the conventional understanding that the primary form of heat extraction is the conduction to the heat sink, instead of the convection.

References

[1] Wolinsky, Howard (February 5, 2005). "U. of I.'s Holonyak out to take some of Edison's luster". Chicago Sun-Times.

[2] W. J. Hwang, T. H. Lee, L. Kim, and M. W. Shin, "Determination of Junction Temperature and Thermal Resistance in the GaN-based LEDs Using Direct Temperature Measurement." *Phys. Stat. Sol.* C 1, No. 10, 2429–2432, 2004.

[3] "In-situ LED Junction Temperature and Thermal Resistance Measurement", *Electronic Systems INC*., Vektrex.

[4] E. Hong, N. Narendran, "A Method for Projecting Useful Life of LED Lighting Systems", *Third International Conference on Solid State Lighting, Proceedings of SPIE,* 5187: 93-99.

[5] M. Farzaneh, K. Maize, D. L¨uerßen, J. A. Summers, P. M. Mayer, P. E. Raad, K. P. Pipe, A. Shakouri, R. J. Ram, and J. A. Hudgings, "CCD-based Thermoreflectance Microscopy: Principles and Applications.", *Journal of Physics D: Applied Physics*, Vol.42, 143001, 20pp, 2009.

[6] M. R. Krames, T. S. Tan, J. Posselt, "High-power Truncated-inverted-pyramid „„$(Al_xGa_{1-x})_{0.5}In_{0.5}P$/GaP lighting emitting diodes Exhibiting $> 50\%$ External Quantum Efficiency.", *Applied Physics Letters*, Vol.75, No. 16, 1999.

[7] http://upload.wikimedia.org/wikipedia/commons/a/a5/Diode-IV-Curve.svg

[8] LUXEON K2 Reliability Datasheet,
http://www.philipslumileds.com/pdfs/RD06.pdf

[9] J. A. Summers, J. A. Hudgings, "Confocal Thermoreflectance for Spatially Resolved Surface Thermography of Transparent LEDs.", *Lasers and electro-Optics and Conference on Quantum electronics and Laser Science Conference*, 2009

[10] B. A. Saleh, M. C. Teich, Fundamentals of Photonics. New York: John Wiley & Sons Inc., 1991.

[11] K. F. Brennan, The Physics of Semiconductors. The Press Syndicate of the University of Cambridge, 1999.

[12] B. V. Zeghbroeck, Principles of Semiconductor Devices. http://www.bookdepository.com/book/9780130409041/Principles-of-Semiconductor-Devices-and-Heterojunctions

[13] Dow Corning, "Material and Solutions to the LED Industry", http://www.dowcorning.com/electronics

[14] Wikipedia: Light-emitting diode http://en.wikipedia.org/wiki/Light-emitting_diode

[15] I. Moreno, D. Bermúdez, and M. Avendaño-Alejo, "Light-emitting diode spherical packages: an equation for the light transmission efficiency." *Applied Optics*, Vol. 49, Issue 1, pp. 12-20, 2010

[16] Wikipedia: Thermal management of high-power LEDs. http://en.wikipedia.org/wiki/Thermal_management_of_high-power_LEDs

[17] http://www.acc-silicones.com/products/encapsulants/applications/leds.ashx

[18] "LED Thermal Management", LED professional, ISSN 1993-890X http://www.led-professional.com/downloads/LpR_13_468932.pdf

[19] E. Narendran, L. Deng, R.R. Pysar, Y. Gu and H. Yu, "Performance Characteristics of High-power Light-emitting Diodes.", Third International Conference on Solid state Lighting, Proceedings of SPIE, 5187:267-275

[20] "New Tools for Thermal Management of LEDs", Alenas Imaging Inc.